*European Journal of Taxonomy* 1004: 144–189
https://doi.org/10.5852/ejt.2025.1004.2973

europeanjournaloftaxonomy.eu
ISSN 2118-9773
2025 · Gooday A.J. *et al.*

*Received: 23 June 2024* • *Accepted: 11 March 2025* • *Published: 22 July 2025*

*Topic editor: Magalie Castelin and Fabio Cianferoni* • *Desk editor: Pepe Fernández*

**Research article**

urn:lsid:zoobank.org:pub:6684E3B8-2E80-425E-AB4C-60829B7CF16B

# Integrative taxonomy of new xenophyophores (Rhizaria, Foraminifera) from the abyssal northwest Pacific

Andrew J. GOODAY[1,*], Yoshiyuki ISHITANI[2], Chong CHEN[3], Maria HOLZMANN[4], Julien RICHIRT[5], Koji SEIKE[6], Momo YAMASHITA[7], Masashi TSUCHIYA[8] & Hidetaka NOMAKI[9]

[1] National Oceanography Centre, European Way, Southampton SO14 3ZH, UK.
[1] Life Sciences Department, Natural History Museum, Cromwell Road, London SW7 5BD, UK.
[2,3,5,9] Institute for Extra-Cutting-Edge Science and Technology Avant-garde Research (X-STAR), Japan Agency for Marine-Earth Science and Technology (JAMSTEC), 2-15 Natsushima-cho, Yokosuka, Kanagawa, 237-0061, Japan.
[4] Department of Genetics and Evolution, University of Geneva, Quai Ernest Ansermet 30, 1211 Geneva 4, Geneva, Switzerland.
[5] Univ. Lille, CNRS, Univ. Littoral Côte d'Opale, IRD, UMR 8187, LOG, Laboratoire d'Océanologie et de Géosciences, Station Marine de Wimereux, 59000, Lille, France.
[6,7] Geological Survey of Japan, National Institute of Advanced Industrial Science and Technology (AIST), Central 7, 1-1-1 Higashi, Tsukuba, Ibaraki 305-8567, Japan.
[6] Department of Natural Environmental Studies, Graduate School of Frontier Sciences, The University of Tokyo, 5-1-5 Kashiwanoha, Kashiwa, Chiba 277-8563, Japan.
[6] School of Science, The University of New South Wales, Northcott Drive, Canberra, ACT, 2600, Australia.
[7] National Museum of Nature and Science, 4-1-1 Amakubo, Tsukuba, Ibaraki 305-0005, Japan.
[8] Research Institute for Global Change (RIGC), Japan Agency for Marine-Earth Science and Technology (JAMSTEC), 2-15 Natsushima-cho, Yokosuka, Kanagawa, 237-0061, Japan.

[*] Corresponding author: ang@noc.ac.uk
[2] Email: ishitaniy@jamstec.go.jp
[3] Email: cchen@jamstec.go.jp
[4] Email: maria.holzmann@unige.ch
[5] Email: richirt.julien@gmail.com
[6] Email: seike-k@aist.go.jp
[7] Email: mmymst@icloud.com
[8] Email: tsuchiyam@jamstec.go.jp
[9] Email: nomakih@jamstec.go.jp

**Abstract.** Xenophyophores dominate the abyssal megafauna across many areas of the Pacific Ocean. These giant agglutinated foraminifera have been studied mainly in the tropics, including within the Clarion-Clipperton Zone (CCZ), from where the majority of recently described taxa have originated. Here, we describe three new species, one of them assigned to a new genus, from an area further north

(30–32.5° N) near the Japanese Archipelago. Specimens were collected in pushcores during dives of the manned submersible *Shinkai 6500* and preserved in the cores after removal of fragments for genetic analyses, allowing them to be examined in life position using X-ray micro-computed tomography (μCT). The three species have basically plate-like tests composed largely of mineral grains. Two, both from 32.5° N, are assigned to the genus *Psammina.* They are closely related to each other and to *P. tenuis* from the western CCZ. In *Psammina yokosukae* sp. nov., the test comprises curved plates, whereas in *Psammina contorta* sp. nov., it comprises a confusing array of contorted plates and other poorly defined structures. The third new species, *Laminarena variabilis* gen. et sp. nov., is genetically distinct from the others. In typical specimens from 30° N, the plates are large, curved or sinuous, relatively thin, and marked by a distinct surface pattern of concentric zones, traversed by closely spaced, radial ridges that correspond to internal partitions. A form from 32.5° N is shown to be conspecific with the 30° N specimens based on molecular evidence but is morphologically more complex, comprising elongate bar- and plate-like elements, some with fan-like terminations. A fourth taxon, resembling a bumpy pebble and occupied by bubble-like internal compartments, is described informally. These new taxa enhance our knowledge of Pacific xenophyophores, as well as our understanding of the morphological diversity of xenophyophores in general.

**Keywords.** Protista, deep sea, benthic megafauna, new species, new genus, micro-CT scanning.

Gooday A.J., Ishitani Y., Chen C., Holzmann M., Richirt J., Seike K., Yamashita M., Tsuchiya M. & Nomaki H. 2025. Integrative taxonomy of new xenophyophores (Rhizaria, Foraminifera) from the abyssal northwest Pacific. *European Journal of Taxonomy* 1004: 144–189. https://doi.org/10.5852/ejt.2025.1004.2973

## Introduction

Xenophyophores are a major component of the abyssal megafauna in many parts of the world, notably so in the Pacific Ocean (Gooday *et al*. 2017a; Simon-Lledó *et al*. 2019a, 2019b, 2019c). These giant agglutinated foraminifera were first collected from the northwest (NW) Pacific in the vicinity of the Japanese Archipelago in 1875 during the *Challenger* expedition and described by Haeckel (1889) as *Psammophyllum flustratum* Haeckel, 1889 and *Psammophyllum annectens* Haeckel, 1889 (= *Stannophyllum flustratum* and *S. zonarium* Haeckel, 1889, respectively; Tendal 1972). Some 80 years later in the 1950s, the Russian research vessel (RV) *Vityaz* obtained further xenophyophore material from off Japan, again belonging to the genus *Stannophyllum* Haeckel, 1889, while members of this genus were also found further north off the Kamchatka Trench and near the Aleutian Trench (Tendal 1972, 1973). The genus *Stannophyllum*, regarded as a sponge by Haeckel, belongs to a morphologically distinct group, the Stannomida Tendal, 1972, in which the test is held together by fine organic fibres. These fibres make the test flexible and able to survive collection in towed samplers such as the trawls that were used during the *Challenger* and other early deep-sea expeditions.

Morphology-based classifications assign xenophyophores other than stannomids to the order Psamminida Tendal, 1972 (Tendal 1972). These have mainly rigid tests and lack organic fibres. Many form delicate, fragile structures that are badly damaged or destroyed in trawls and can only be recovered intact in box cores or multicores unless a submersible is used (Tendal 1996). Most of the species described in recent years are of this type. The first to be discovered in the NW Pacific near Japan was *Occultammina profunda* Tendal, Swinbanks, Shirayama, 1982, described by Tendal *et al.* (1982) from a hadal site (8260 m) in the Ogasawara Trench near Ogasawara Islands (see also Swinbanks & Shirayama 1986a, 1986b). In the same year, a similar unnamed species was reported from 6440 m in the Japan Trench by Swinbanks (1982). The next important contribution was the description by Lecroq *et al.* (2009) of a new genus and species, *Shinkaiya lindsayi* Lecroq, Gooday, Tsuchiya & Pawlowski, 2009, from the abyssal plain off Sanriku, northern part of Japan. Hori *et al.* (2013) analysed bacteria associated with

an unnamed xenophyophore, genetically close to *S. lindsayi*, from the Izu-Ogasawara Trench (7111 m depth). Recently, Tsuchiya & Nomaki (2021) conducted in situ seafloor feeding experiments with two xenophyophores at a site (5370 m) off the east coast of Torishima Island. Abyssal xenophyophores have also been observed in seafloor photographs taken near Japan (e.g., Fujioka *et al.* 1989). Finally, Voltski *et al.* (2018) described a new species, *Syringammina limosa* Voltski, Weiner, Tsuchiya & Kitazato, 2018, from lower bathyal depths (3351–3366 m) in the Sea of Okhotsk to the north of the Japanese Islands.

More is known about xenophyophores in the abyssal equatorial Pacific, well to the south and east of the Japanese Archipelago. Their importance in this region was already recognised by early researchers, notably Schultze (1907). During the last decade, a large effort has been devoted to studying the Clarion-Clipperton Zone (CCZ), a region of the equatorial Pacific hosting vast seafloor deposits of polymetallic nodules of considerable commercial interest. Here, xenophyophores are often the dominant component of the megafauna in seafloor images (Kamenskaya *et al.* 2013; Amon *et al*. 2016; Simon-Lledó *et al*. 2019a, 2019b, 2019c). This has led to the description of 22 new species and six new genera as well as the recognition of a larger number (currently 44) of undescribed forms (reviewed in Gooday *et al.* 2017a, 2020b; see also Gooday & Wawrzyniak-Wydrowska 2023).

The present study builds on this previous research in the vicinity of Japan and in the CCZ. We use a combination of light photography, scanning electron microscopy (SEM), and X-ray micro-computed tomography (μCT) to comprehensively characterise the external and internal test morphology of the three new species and a new genus, with the descriptions being supported by genetic data.

## Material and methods

### Sampling and processing of xenophyophores

Xenophyophores were collected during several cruises of the RV *Yokosuka* at two soft-sediment abyssal plain sites; 30° N (30°09.2′ N, 143°35.1′ E, water depth 5366 m: Tsuchiya & Nomaki 2021) and 32.5° N (32°34.8′ N, 143°46.2′ E, water depth 5505 m) (Table 1; Supp. file 2: Fig. S1). There are no obvious topographic features, such as depressions, hills or ridges, that could influence faunal composition and abundance (Durden *et al*. 2015; Stefanoudis *et al*. 2016; Simon-Lledó *et al.* 2019b) in the vicinity of these sampling sites (Supp. file 2: Figs S2–S3).

Specimens were collected during dives of the human-occupied vehicle (HOV) *Shinkai 6500*. We used a push corer with an inner diameter of 82 mm and core tube lengths of 320 mm, which retained the underlying sediment as well as the xenophyophores. Upon recovery, sediment cores were stored in a cold room (4°C) and then processed as follows. After taking photographs, fragments (typically 1 to 2 cm in size) were gently removed and fixed with either 2.5% glutaraldehyde/filtered seawater or RNAlater solution (Qiagen). A second core tube with the same diameter as the pushcore tube (i.e., inner diameter 82 mm, outer diameter 89 mm, length ca 200 mm) was then placed on the top of the pushcore tube and connected to it securely with vinyl tape. The overlying water, the xenophyophore, and soft sediment below it, were gently extruded into the upper tube and the bottom of the tube secured with a silicon rubber plug. The overlying water was fixed with 10% formalin buffered with sodium tetraborate and the top of the tube was sealed with another silicon rubber plug, secured with vinyl tape.

Type and other specimens are preserved in core tubes with 10% buffered formalin, are deposited in the National Museum of Nature and Science, Tsukuba (TNS), Japan.

### Light photography

Most of the light photography was done at the Japan Agency for Marine-Earth Science and Technology (JAMSTEC, Yokosuka, Japan) using an Olympus Tough Model IM015 digital camera, either handheld or attached to a Nikon SM218 stereo microscope. Other photographs were taken at the University of

**Table 1.** Station and species details. In column 10 H = Holotype, P = Paratype, NT = Non-type. The registration numbers in column 11 are for individual specimens and were assigned by the National Museum of Nature and Science, Tsukuba (TNS), Japan. Supplementary figures (S1–S14) see Supp. file 2.

| Station | Dive | Core | Lat. °N | Long. °E | Depth (m) | Species | Isolate | GenBank | Type | Reg. nos. | Figures |
|---|---|---|---|---|---|---|---|---|---|---|---|
| 30N | 1660 | Blue#1 | 30º09.18′ | 143º35.12′ | 5366 | *L variabilis* | N/A | N/A | P | TNS-Pr699 | 12–13, 16, S6 |
| 30N | 1660 | Blue#2 | 30º09.18′ | 143º35.12′ | 5366 | *L variabilis* | 21948 | PP662670 | H | TNS-Pr700 | 11, S6 |
| 30N | 1660 | Blue#6 | 30º09.18′ | 143º35.12′ | 5366 | *L variabilis* | N/A | N/A | NT | TNS-Pr702 | 14, S6, S8 |
| 30N | 1660 | Blue#7 | 30º09.18′ | 143º35.12′ | 5366 | *L variabilis* | N/A | N/A | NT | TNS-Pr703 | S6, S9, S14 |
| 30N | 1660 | Red#4 | 30º09.18′ | 143º35.12′ | 5366 | *L variabilis* | N/A | N/A | NT | TNS-Pr705 | 14–15, 21, S6–S7 |
| 32.5N | 1659 | Red#3 | 32º34.81′ | 143º46.24′ | 5509 | *P. yokosukae* | 21945-21947 | PP662675–PP662677 | H | TNS-Pr691 | 2–5, 8, S4–S5 |
| 32.5N | 1659 | Red#5 | 32º34.79′ | 143º46.12′ | 5509 | *P. yokosukae* | 21935, 21938 | PP662673, PP662674 | P | TNS-Pr693 | 2, 6–7, S4 |
| 32.5N | 1659 | Red#7 | 32º34.81′ | 143º46.24′ | 5509 | *P. contorta* | 21955 | PP662680 | P | TNS-Pr694 | 2, 5, 8, 10, 22, S4–S5 |
| 32.5N | 1659 | Red#8 | 32º34.81′ | 143º46.24′ | 5509 | *P. contorta* | 21950, 21951 | PP662678, PP662679 | H | TNS-Pr695 | 2, 5, 9, S4–S5 |
| 32.5N | 1659 | Red#9 | 32º34.81′ | 143º46.25′ | 5509 | *L variabilis* | 21953, 21954 | PP662671 PP662672 | NT | TNS-Pr697 | 17–19, 21–22, S10, S14 |
| 32.5N | 1691 | Blue#0 | 32º34.66′ | 143º46.14′ | 5505 | *L variabilis* | 6K1691_B0a 6K1691_B0b | PP741523-26 PP741527-31 | NT | TNS-Pr714 | 17–19, S10–S11, S13 |
| 32.5N | 1633 | Blue#1 | 32º34.71′ | 143º46.14′ | 5509 | *L variabilis* | N/A | N/A | NT | TNS-Pr690 | S10, S12 |
| 32.5N | 1659 | Red#8 | 32º34.81′ | 143º46.24′ | 5509 | Honeyombe pebble | N/A | N/A | NT | TNS-Pr696 | 9, 20, 22 |

Geneva (Switzerland), mainly of test fragments and granellare (the cytoplasm and its tubular sheath) during the preparation of extractions for molecular analyses, using a Leica M205 C motorized stereo microscope equipped with a Leica DFC 450 C camera. A few additional photographs of test fragments were taken at the National Oceanography Centre (NOC, Southampton, UK) using an Olympus SZX7 stereo microscope and an Olympus BH2 compound microscope, both equipped with a Canon 60D SRL digital camera.

**Scanning electron microscopy**

Scanning electron microscopy (SEM) was performed using two different microscopes at JAMSTEC. SEM imaging and energy-dispersive X-ray spectroscopy (EDS) analyses were performed with a Quanta FEG 450 (Thermo Fisher Scientific Inc.) equipped with an EDS detector (Octane Elite Plus, AMETEC, Inc.). Samples were first mounted onto an aluminium stub (Ø 10 mm) using double-sided carbon tape and coated with Os at 15 nm using an OS plasma coater OPC80 (Filgen). Secondary electron (SE) images were collected using an Everhart-Thornley detector at 2 to 10 kV acceleration voltage. EDS analyses were performed at an acceleration voltage of 10 kV. Additional images were obtained with a benchtop SEM (JEOL JCM-6000Plus) in low vacuum mode at 15 kV of acceleration voltage and using backscattered electron mode (BSE).

**X-ray µCT analyses**

Sediment cores, including the xenophyophores, were scanned and observed using a micro-computed tomography (µCT) system (inspeXio SMX-22-225CT FPD, Shimadzu Corporation, Kyoto, Japan) at the National Museum of Nature and Science in Tsukuba, Japan. Scans were performed at 200 kV and 70 µA, with voxel resolutions of images varying from 0.082 to 0.103 mm. The µCT data were visualized and analyzed using the 3D rendering function in the software Amira3D Pro ver. 2022.2 (Thermo Fisher Scientific, USA) installed at JAMSTEC (Japan). Where applicable, granellare strands were segmented using the threshold function and rendered as 3D surface for display. All image captures and measurements were made in orthogonal view.

**DNA extraction, PCR amplification and sequencing**

Twenty DNA extractions were obtained from the three xenophyophore species using the DNeasy Plant Mini Kit (Qiagen). Semi-nested PCR amplification was carried out for the 18S rRNA barcoding fragment of foraminifera (Pawlowski & Holzmann 2014) using forward primers s14F3 (5′acgcamgtgtgaaacttg3′) -s20r (5′gacgggcggtgtgtacaa3′) for the first and primers s14F1 (5′aagggcaccacaagaacgc3′)-s20r for the second amplification. Thirty-five and 25 cycles were performed for the first and the second PCR, with an annealing temperature of 50°C and 52°C, respectively (Holzmann 2024). The amplified PCR products were purified using the Roti®Prep PCR Purification Kit (Roth). Two PCR-amplified DNA fragments (isolates 6K1691_B0a and 6K1691_B0b) were cloned into the pCR21-TOPO vector using the TOPO TA cloning Kit (Invitrogen). Eight clones were sequenced for each amplified isolate. Sequencing reactions were performed using the BigDye Terminator ver. 3.1 Cycle Sequencing Kit (Applied Biosystems) and analyzed on a 3130XL Genetic Analyzer (Applied Biosystems). The resulting sequences were deposited in the NCBI/GenBank database. Isolate and accession numbers are listed in Supp. file 1.

**Phylogenetic analysis**

The obtained sequences were added to 47 monothalamid sequences (Supp. file 1) that are part of the publicly available 18S database (NCBI/Nucleotide; www.ncbi.nlm.nih.gov/nucleotide/). All sequences were aligned using the default parameters of the Muscle automatic alignment option as implemented in SeaView ver. 4.3.3. (Gouy *et al*. 2010). The alignment contains 79 untrimmed sequences with 1113 sites used for analysis. The phylogenetic trees (Fig. 1) were constructed using maximum likelihood phylogeny by PhyML 3.0 as implemented in ATGC: PhyML (Guindon *et al*. 2010), available online at http://www.atgc-montpellier.fr/phyml (last accessed 16 May 2024). An automatic model selection by

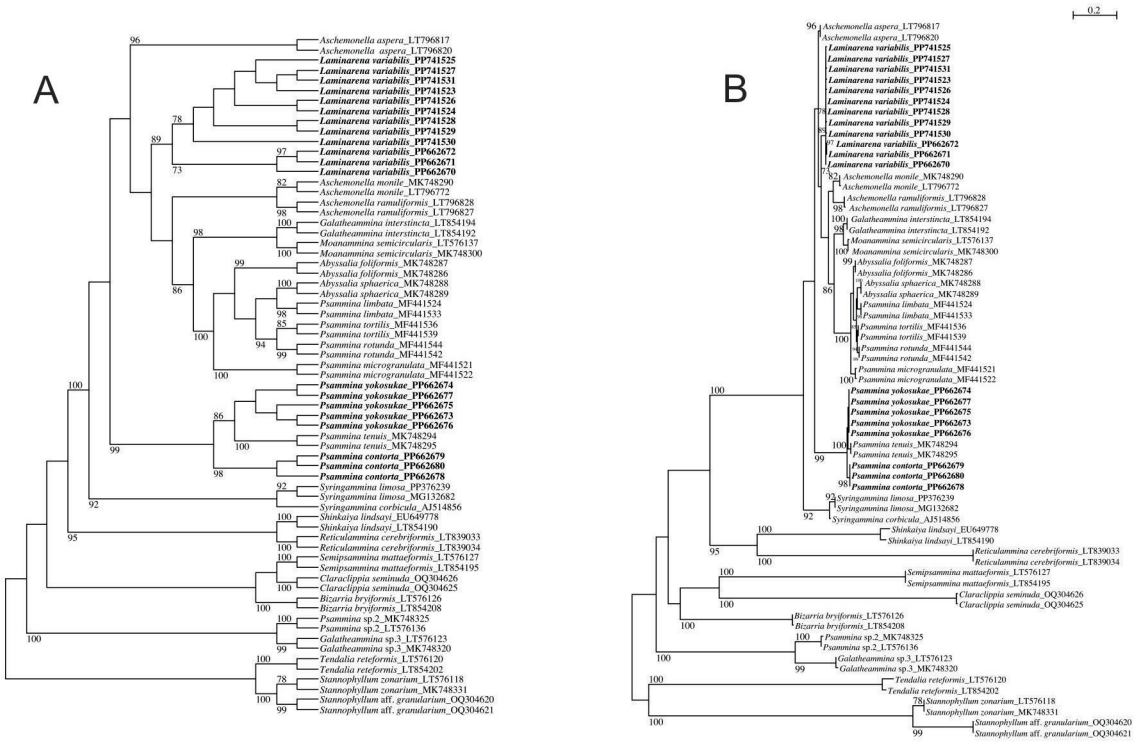


**Fig. 1.** PhyML phylogenetic trees based on the 3′ end fragment of the SSU rRNA gene, showing the evolutionary relationships of 67 foraminiferal sequences belonging to monothalamids. Specimens marked in bold indicate those for which sequences were acquired during the present study. The trees are unrooted. Specimens are identified by their accession numbers. Numbers at nodes indicate bootstrap values (BVs). Only BVs >70% are shown. **A**. Cladogram. **B**. Phylogram.

Smart Model Selection (SMS, Lefort *et al*. 2017) based on Akaike Information Criterion (AIC) was used, resulting in a GTR+G substitution model being selected for the analysis. The initial tree is based on BioNJ and bootstrap values (BV) are based on 100 replicates.

## Results

### *Taxonomy*

Rhizaria Cavalier-Smith, 2002
Retaria Cavalier-Smith, 1999
Foraminifera D'Orbigny, 1826
Monothalamea Pawlowski, Holzmann & Tyszka, 2013
Xenophyophoroidea Tendal, 1972

Genus ***Psammina*** Haeckel, 1889

***Psammina yokosukae*** sp. nov.
urn:lsid:zoobank.org:act:8F06D3F4-DE75-46FD-8701-0D6C1379EB9E
Figs 2A–B, 3–4, 5D–G, 6–7, 8A–E; Supp. file 2: Figs S4A–B, S5A–B, Supp. file 3: µCT video 1

#### Diagnosis

Species of *Psammina* with free, epifaunal test comprising system of undulating, sometimes fan-shaped, plates up to >5 cm in overall extent. In places, surface displays vague concentric zones defined by

slightly raised lineations and traversed by low radial ridges. Micro-CT scans reveal internal structures, often rather poorly defined, corresponding to these surface features. Obvious apertures absent. Test wall friable, comprising mineral grains of varying sizes (generally <100 μm) and occasional biogenic particles. Interior partly filled with agglutinated mineral grains that are larger (>300 μm) than those constituting the wall. Stercomare forms branching and anastomosing strings and masses of variable width (~70 to >200 μm) that occupy spaces between internal grains with no clear pattern. Granellare yellowish-brown, branching, thread-like (width ~10 to 34 μm), in places attached to grain surfaces; barite crystals rare.

**Etymology**

Named for the RV *Yokosuka*, support ship for the HOV *Shinkai 6500.*

**Material examined**

**Holotype**

NW PACIFIC OCEAN – **32.5° N (west of Kuroshio Extension Observatory (KEO))** • 32°34.81′ N, 143°46.24′ E; depth 5509 m; 22 Oct. 2022; H. Nomaki leg.; Dive 1659 of HOV *Shinkai 6500*, core Red#3; GenBank accession nos: PP662675 to PP662677; National Museum of Nature and Science, Tsukuba, Japan, reg. no. TNS Pr691. The specimen is preserved in a core in 10% buffered formalin.

**Paratype**

NW PACIFIC OCEAN – **32.5° N (west of KEO)** • 1 spec.; same data as for holotype; Dive 1659 of HOV *Shinkai 6500*, core Red#5; National Museum of Nature and Science, Tsukuba, Japan, reg. no. TNS Pr691. The specimen was frozen at sea and only available as fragments.

**Description**

**Overall test morphology**

The in situ seafloor photograph of the holotype (Fig. 2A) shows a group of about five main plate-like elements that are curved or undulating with sinuous and often upturned margins. The plates are orientated in different directions but merge together into one structure. Near one end of the test, there is an open-ended, chimney-like feature that is also visible in the shipboard photograph (Supp. file 2: Fig. S4A). The seafloor photograph of the paratype (TNS Pr693) is similar, although it comprises fewer, relatively larger plates (Fig. 2B).

The recovered holotype measures 5.5 cm × 3.7 cm in maximum extent when viewed from above (Fig. 3B) and extends ~2.7 cm above the sediment surface. The test is composed of plates that are ~0.60–1.0 mm (mean 0.81 ± 0.11 mm, n = 11) thick. It is strongly asymmetrical, with one side low lying, or even slightly buried under resedimented material (Figs 3A–B, 4C–D, G–H), and the other side upstanding. Supp. file 3: μCT video 1 gives a clear impression of its structure. The low-lying side comprises two mainly separate plates with strongly upturned rims. These, and particularly the larger of the two, merge with, and to some extent buttress, the more prominent upstanding part of the test. This part can be thought of as comprising two components. One is a branched plate, the upper part of which forms a U-shaped trough with undulating side (Fig. 3A, E). One side of the trough merges with the second component, a fairly flat semicircular fan that is a visually conspicuous feature in Figs 3C, 4A–D, and shown in detail in Fig. 3D–G. In side view, the fan appears to be linked with the above-mentioned tubular chimney-like structure (Fig. 3A–C, G), but the μCT video (Supp. file 3) clearly shows that this feature develops at the end of one side of the U-shaped trough, after it has merged with the fan-shaped plate. Another approximately circular, somewhat larger but less regular feature is located in the central part of the test. It is largely obscured by other test elements but can be seen at a few points in the video.

**Surface ornamentation, test structure and composition**

In light photographs of the holotype, the test surface displays a vague pattern of concentric zones. These can be seen most clearly under very oblique lighting, notably on the prominent semicircular plate (Fig. 3G; Supp. file 2: Fig. S5B). Where the boundaries between the zones are most clearly developed (Fig. 3G), they appear to be shallow steps, suggesting that later zones overlap earlier ones. Superimposed on these zones are low radial ridges separated by shallow furrows, which are equally indistinct. The same pattern is clearer in µCT images of the holotype than in visible light. When the test is rendered more transparent in µCT scans, it is almost entirely occupied by concentric zones and radial features. Although the pattern of lineations is obvious on the semicircular plate (Fig. 3C–D), the individual features are often indistinct and discontinuous.

The test wall is fairly friable, 180–320 µm (mean 267 ± 56 µm, n = 15) thick, and light greyish in colour when dry. It is continuous around the margin and devoid of obvious apertures. Seen through the wall of the core tube, the surface is peppered with a variable density of larger grains (Fig. 3F–G; Supp. file 2: Fig. S5B). Under a stereo microscope, the surface appears noticeably granular and comprises a rather heterogeneous mixture of mineral grains of various sizes (Fig. 5D, F). Some larger ones are dark and there is a sprinkling of whitish and orange grains, but most are pale or transparent.

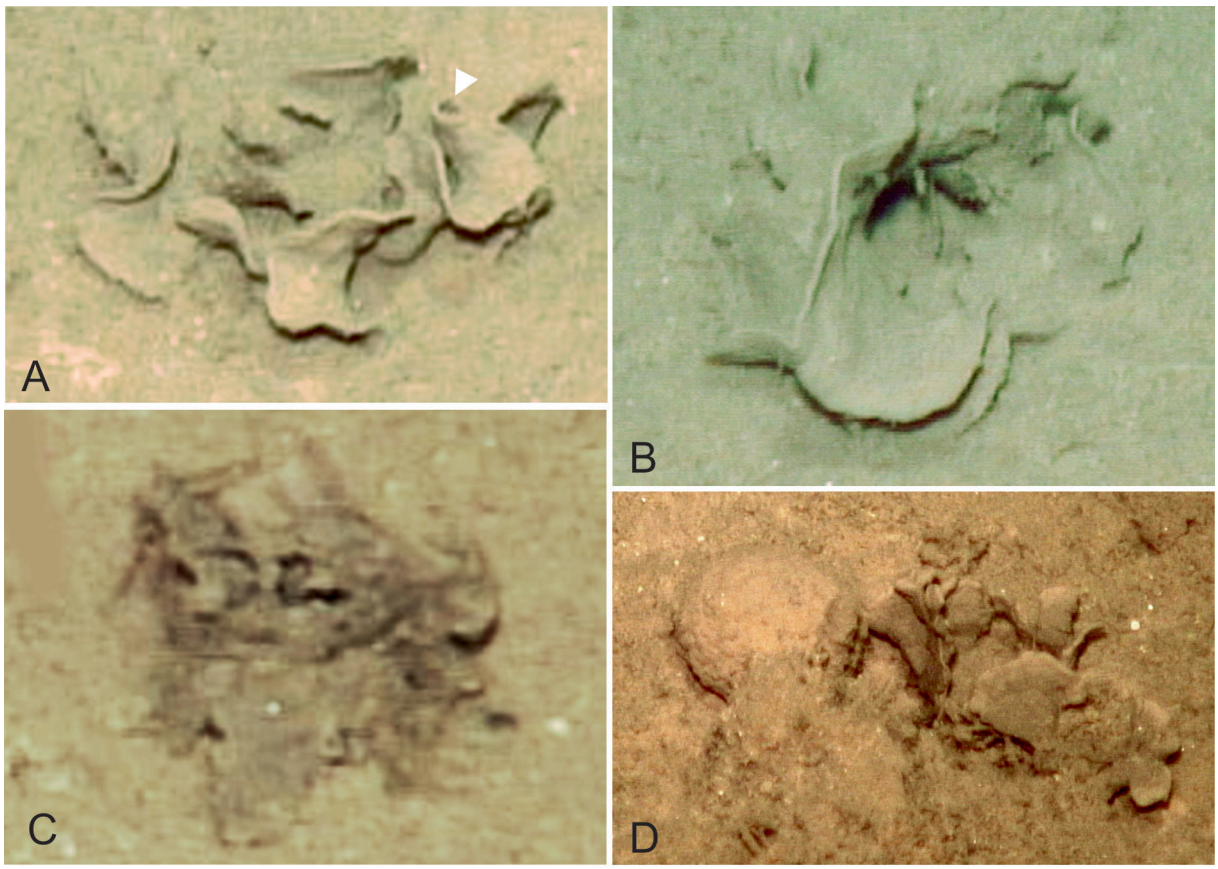


**Fig. 2.** Seafloor images. **A–B**. *Psammina yokosukae* sp. nov. **A**. Holotype, reg. no. TNS Pr691. **B**. Paratype, reg. no. TNS Pr693. **C–D**. *Psammina contorta* sp. nov. **C**. Paratype, reg. no. TNS Pr694. **D**. Holotype, reg. no. TNS Pr695; the rounded object on the left side is the 'Pebble-shaped, honeycombed xenophyophore' informally described below. The arrowhead (A) indicates the chimney-like feature referred to in the text.

In SEM images of the paratype, the surface is quite uneven at a scale of 100–200 μm (Fig. 6A–D). The main constituents are mineral grains amongst which are scattered some biogenic remains. mainly radiolarian fragments, but also diatom fragments. The outer wall is not sharply delimited from the test interior (Fig. 6G). In addition to empty space, the interior is occupied by a variety of particles ('internal xenophyae') of different shapes and sizes that are dominated visually (although not numerically) by grains that are larger (200–300 μm) than those forming the outer layer (Fig. 7A–D). These include sharp-edged shards of volcanic glass, and porous and fibrous particles, possibly also of volcanic origin, in addition to radiolarian fragments.

The relatively few test fragments in which the interior was examined directly did not display well-defined partitions corresponding to the internal structures visible in μCT renders (Fig. 3C–D). However, two or perhaps three poorly-defined internal partitions can be seen in an SEM image showing the interior exposed at the edge of a test fragment (Fig. 6A); a broken cross section of the test shows similar features (Fig. 6G). Vague radial structures are sometimes also discernible when the test interior is viewed by light microscopy (Fig. 5E). The poorly defined nature of these features probably reflects the fact that the internal agglutination is dominated bys coarse-grained particles. This probably also explains why individual radial features are sometimes indistinct and discontinuous in μCT renders (Fig. 3D).

**Stercomare and granellare**

In addition to internal particles, the test contains stercomare and granellare. The dark stercomare forms branches that to some extent anastomose, as well as more irregular masses (Figs 5G, 6F, 8A). At least in the test fragments examined, they did not follow any clear trend but occupied the irregular spaces between the large internal xenophyae. The branches vary greatly in width, from ~70 μm to more than 200 μm. They have a thin, transparent organic sheath, ~1 μm thick, that encloses masses of spherical to ovoid stercomata, each stercome ranging in size from 12 to 30 μm (typically 12–20 μm) (Figs 5G, 6H).

The granellare forms narrow thread-like strings, yellowish-brown in colour (a darker golden-brown when dried), that branch throughout the test interior (Figs 5G, 7A–D, 8A). They measure 10–40 μm in width (usually 14–25 μm; mean 20.7 ± 6.17 μm, n=50) and occupy only a very small proportion of the interior space. The branches weave between the internal xenophyae and in places are attached to the surfaces of grains, from which they are difficult to dislodge. The organic sheath that surrounds the cytoplasm is ~0.1–0.2 μm thick and shrinks creating longitudinal wrinkles when dried on an SEM stub (Fig. 7E). Granellare fragments viewed in glycerol under a compound microscope show the cytoplasm with small inclusions of various kinds, including a few refractive particles that are presumably mineral grains (Fig. 8D–E), although these do not resemble typical barite crystals. There was little evidence for intracellular barite crystals in SEM images. None were visible through the granellare walls (Fig. 7E). Various inclusions could be seen within the cytoplasm where the granellare tube was ruptured, but only a single crystal-like particle yielded EDS peaks for Ba (Fig. 7H), suggesting that barite crystals are not common**.**

**Molecular characterisation**

*Psammina yokosukae* sp. nov. branches as sister to *Psammina tenuis* Gooday & Holzmann, 2020. The grouping is supported by a BV of 89%. The sequenced fragment of the 18S gene of *P. yokosukae* contains 1038–1039 nucleotides and the GC content is 36 %.

**Remarks**

Phylogenetic reconstruction shows that *Psammina yokosukae* sp. nov. is closely related to *P. tenuis*. In terms of morphology, the granellare branches of both species are similar in being narrow (*P. yokosukae* 12–22 μm; *P. tenuis* 10–30 μm) and attached for part of their length to internal test particles. The two species are also similar in having basically plate-like tests. An in situ photograph of the unique specimen of *P. tenuis* on the seafloor shows a relatively simple plate, strongly curved around a vertical axis,

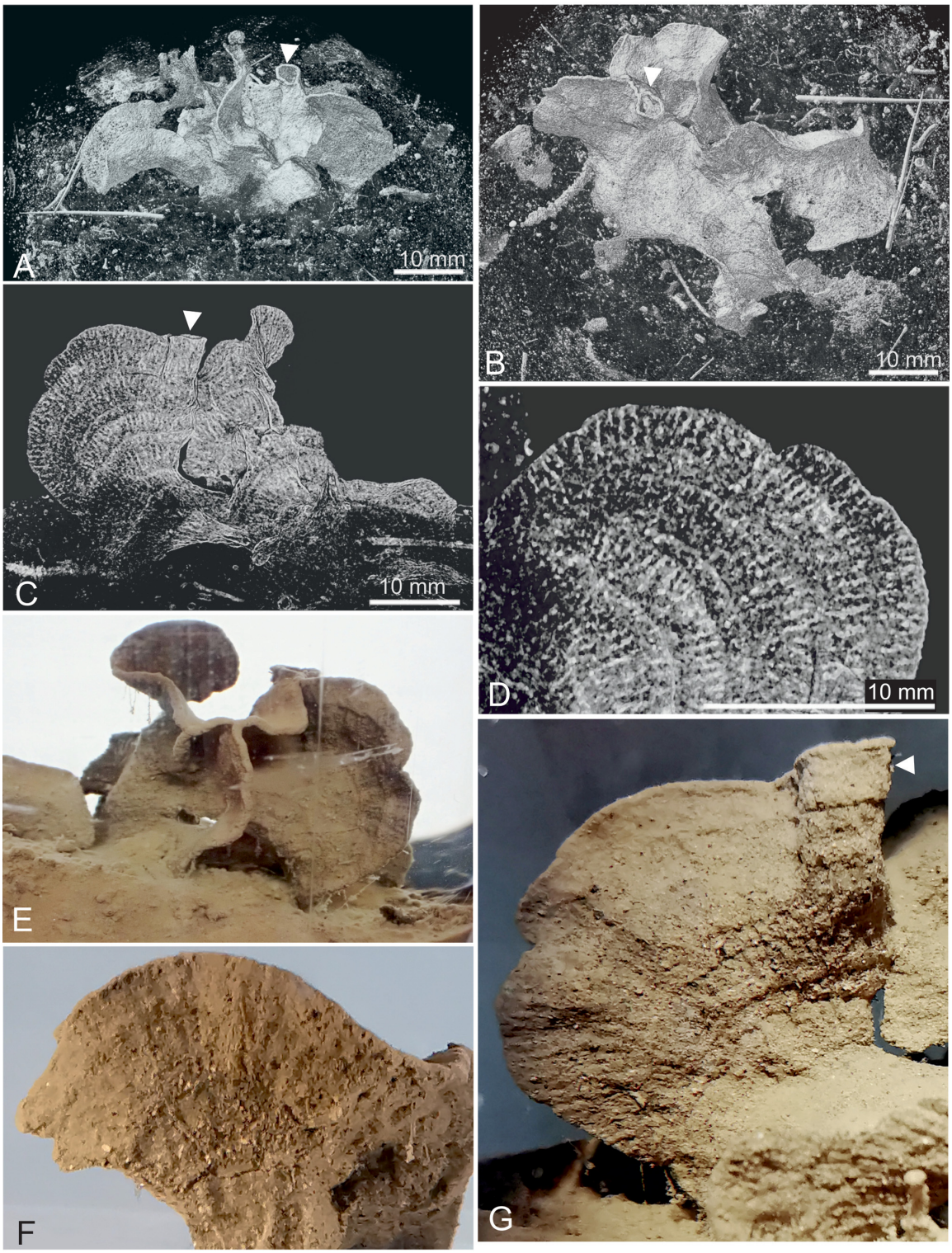


**Fig. 3.** *Psammina yokosukae* sp. nov., holotype, reg. no. TNS Pr691. **A–D**. Micro-CT renders showing surface structures (A–B) and inner structures (C–D) of the test on the core surface. **A**. Oblique view from above. **B**. View from directly above. **C**. Side view showing concentric zones traversed by radial features. **D**. Detail of largest fan-shaped plate. **E–G**. Light photographs taken through the side of the plastic core tube. **E**. Main upstanding part of test. **F–G**. Two plates with concentric zones and low radial ridges. The arrowheads (A–C, G) indicate the chimney-like feature referred to in the text.

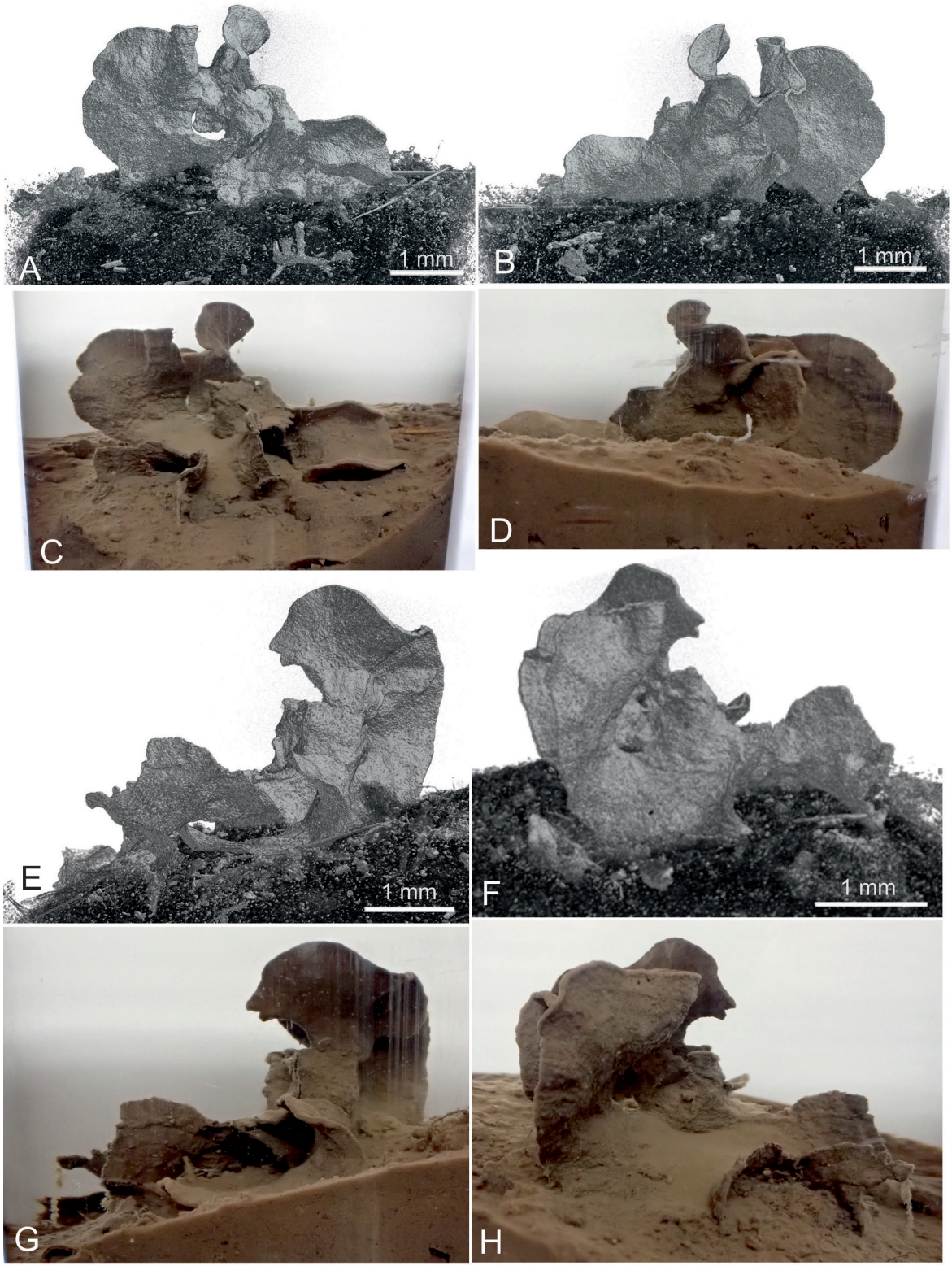


**Fig. 4.** *Psammina yokosukae* sp. nov., holotype, reg. no. TNS Pr691. **A–B, E–F**. Micro-CT renders of complete test from different angles, showing surface structure. **C–D, G–H**. Corresponding light photographs taken through the side of the plastic core tube; note optical distortion due to curvature of tube wall.

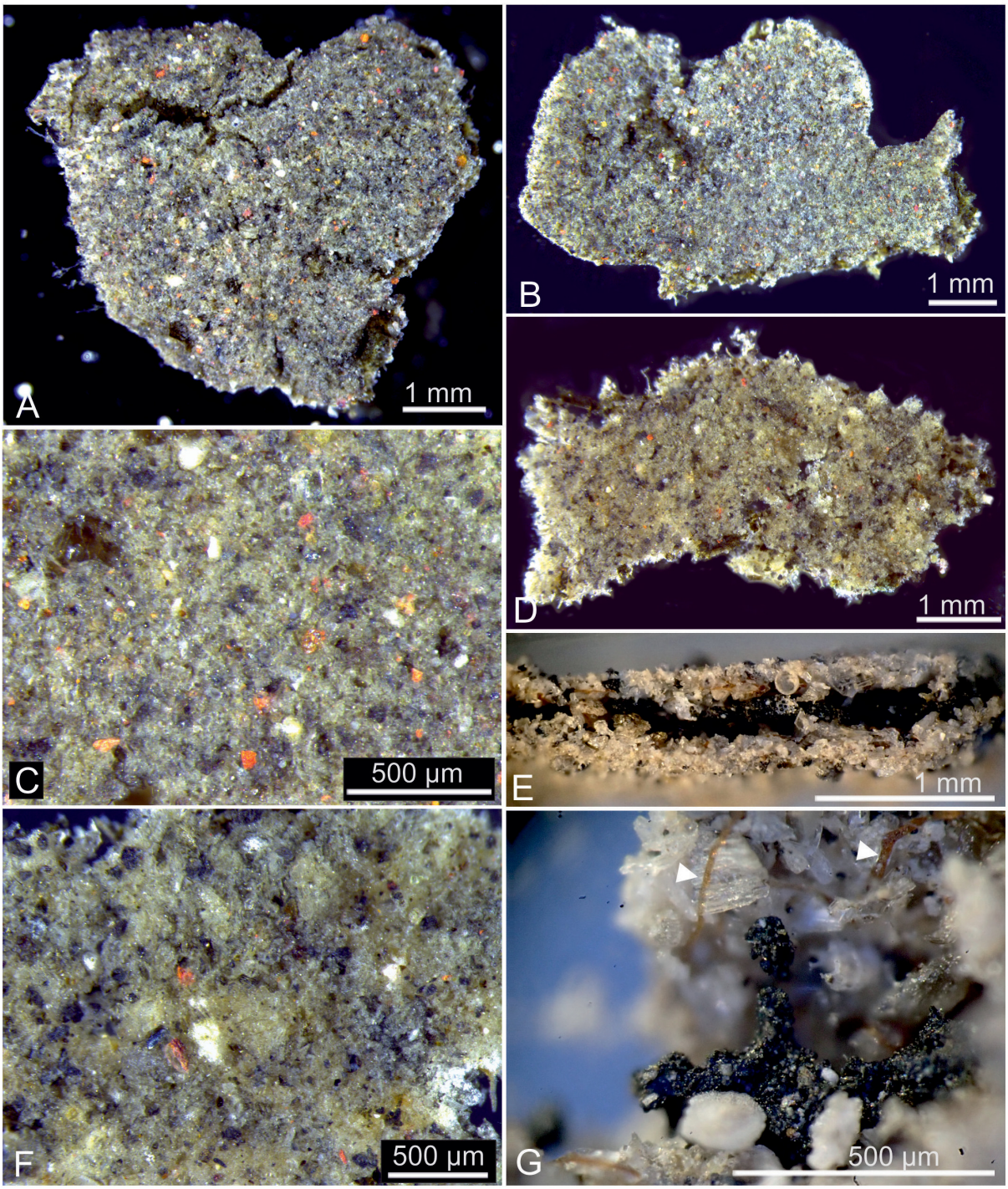


**Fig. 5.** Stereo microscope images. **A–C**. *Psammina contorta* sp. nov. **A**. Fragment of holotype, reg. no. TNS Pr695. **B**. Fragment of paratype, reg. no. TNS Pr694. **C**. Detail of holotype surface. **D–G**. *Psammina yokosukae* sp. nov., fragments of holotype, reg. no. TNS Pr691. **D**. Outer surface of fragment. **E**. View of broken test edge showing wall and interior with dark stercomare. **F**. Closer view of test wall. **G**. Interior of fragment showing dark stercomare mass comprising accumulation of stercomata (tiny waste pellets) and two thin granellare branches (arrowed). A–D, F taken in Geneva; E, G taken at JAMSTEC.

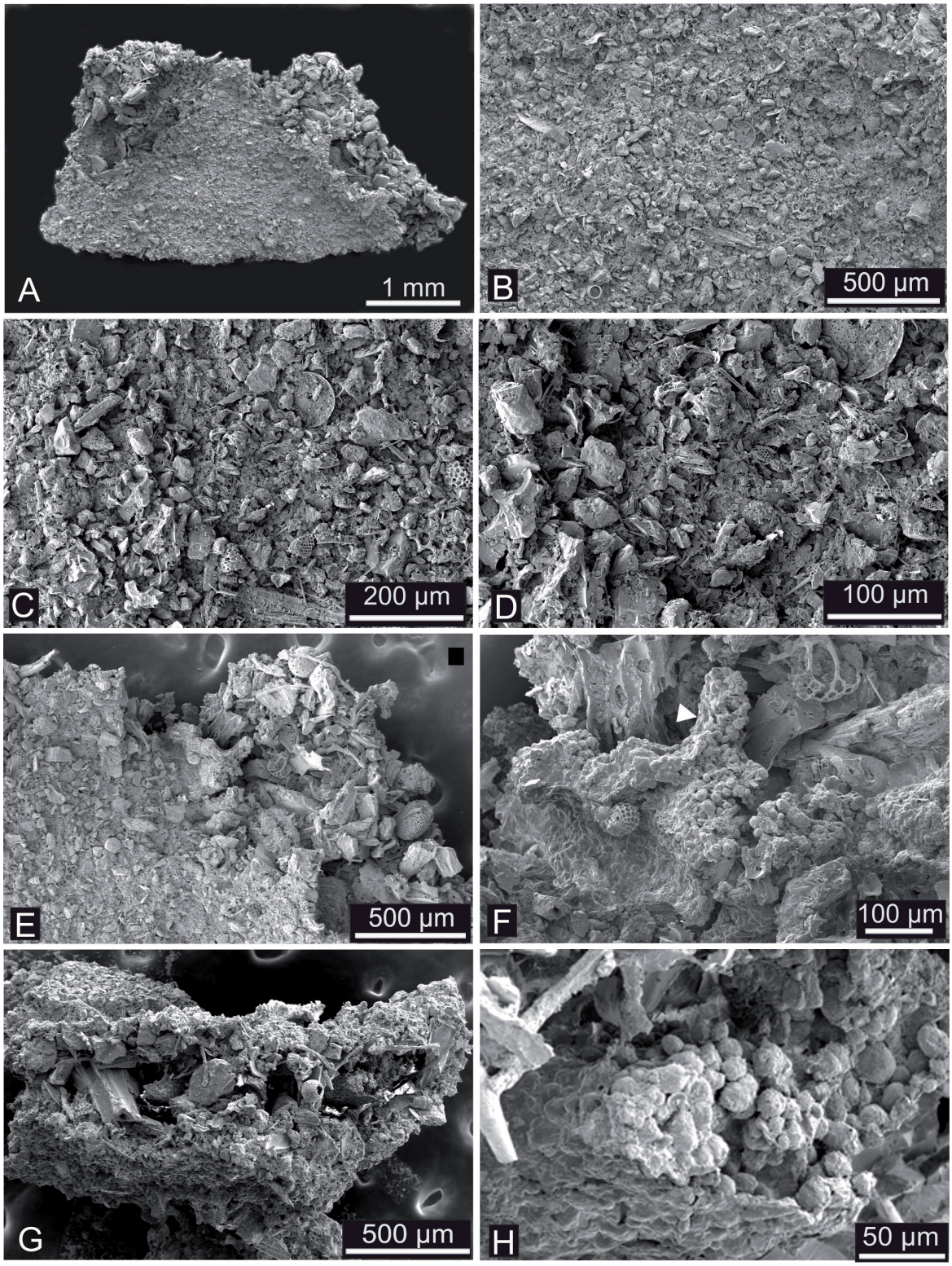


**Fig. 6.** *Psammina yokosukae* sp. nov., SEM images (secondary electron mode) of fragment of paratype, reg. no. TNS Pr693. **A**. Entire test fragment showing outer surface with interior exposed at the edge. **B–D**. Progressively closer views of test surface. **E**. Detail showing outer surface of test and coarser-grained internal surface. **F**. Internal surface showing stercomare (arrowed). **G**. Broken showing vague internal partitions. **H**. Detail of stercomare showing stercomata and enclosing membrane.

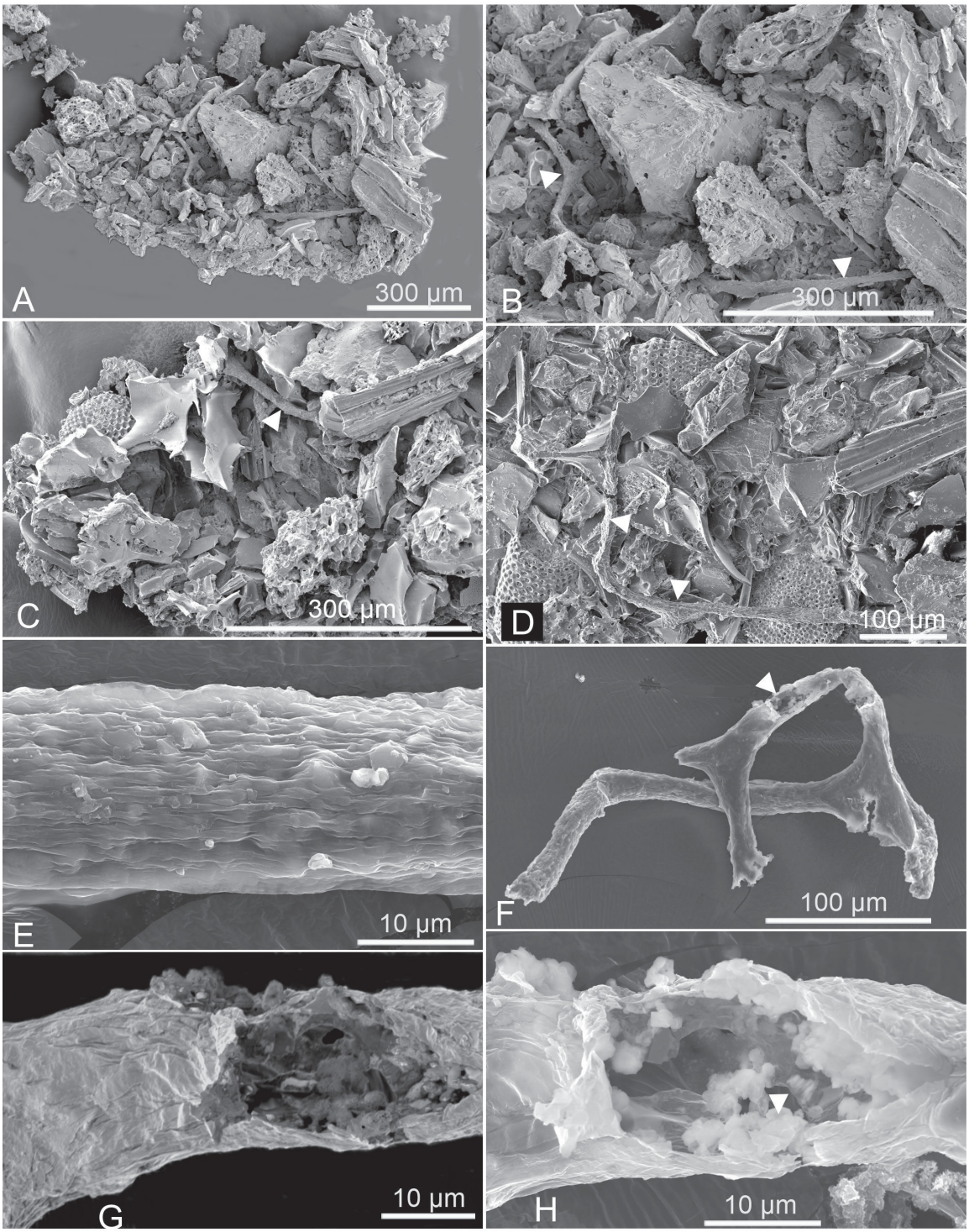


**Fig. 7.** *Psammina yokosukae* sp. nov., SEM images (secondary electron mode) of fragment of paratype, reg. no. TNS Pr693. **A**. Entire test fragment showing inner surface. **B**. Closer views of inner surface. **C–D**. Closer views of two other fragments. **E–H**. Granellare. **E**. Surface of granellare showing crinkled surface of organic tube. **F**. Fragment with ruptured part indicated by arrowhead. **G**. Detail of ruptured granellare showing thin organic tube and heterogeneous contents. **H**. Detail of ruptured granellare showing interior with inclusions, including a crystal (arrowed) that yielded an EDX peak for Ba. Arrowheads in B–D indicate granellare strands.

growing up vertically from the surface of a polymetallic nodule (Gooday *et al*. 2020a: fig. 5a therein). This is somewhat reminiscent of the holotype of *P. yokosukae* but is much simpler than the cluster of plates that make up the test of the new species. Concentric lines are more clearly developed in *P. tenuis* than in *P. yokosukae*, but there is no sign of the radial lineations that are dimly visible in the new species.

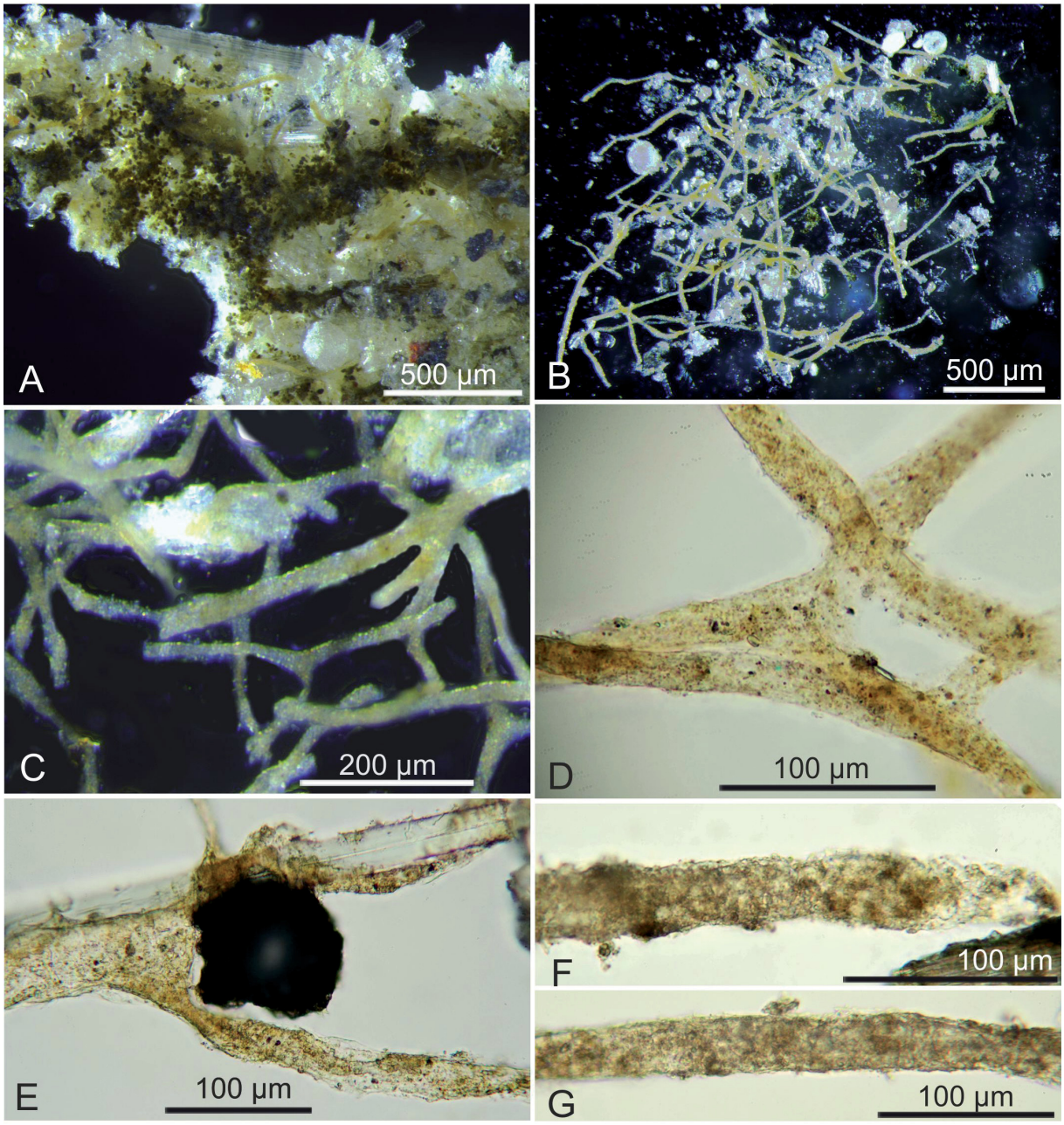


**Fig. 8.** Light microscope images. **A–E**. *Psammina yokosukae* sp. nov., fragments of holotype, reg. no. TNS Pr691. **A**. Test interior showing damaged stercomare; fine granellare strands also visible. **B**. Granellare fragments dissected from test for molecular analyses. **C**. Closer view of granellare fragments. **D–E**. Granellare fragments immersed in glycerol on a glass slide and viewed with transmitted light in compound microscope. **F–G**. *Psammina contorta* sp. nov., granellare fragments from paratype, reg. no. TNS Pr694, viewed in glycerol, as described for D–E. Images A–C were taken in Geneva, D–G in Southampton.

These differences in test morphology support the genetic distinction between *P. yokosukae* sp. nov. and *P. tenuis*. Given the variability of many xenophyophores, an important caveat is that the overall test morphology is known in detail for only one specimen of both species. Nevertheless, the fact that the test wall is composed largely of radiolarian shells in *P. tenuis* but largely of mineral grains in *P. yokosukae*, and the presence of more numerous internal particles in *P. yokosukae*, supports the conclusion that these are different species.

***Psammina contorta*** sp. nov.
urn:lsid:zoobank.org:act:E698FACF-6DE6-461F-95F3-EA971F1F8695
Figs 2C–D, 5A–C, 8F–G, 9–10, 22B; Supp. file 2: Figs S4C–D, S5C–F; Supp. file 4: µCT video 2

**Diagnosis**

Species of *Psammina* with free, epifaunal test comprising complex, irregular system of variously shaped, often crookedly curved, plate-like elements up to ~60 mm in overall extent with no clear growth pattern or symmetry. Obvious apertures absent. Concentric zones sometimes present. Micro-CT scans reveal irregularly shaped, cell-like internal compartments. Test wall friable, comprising mixture of mineral grains of different sizes and colours. Stercomare forms branching and anastomosing strings of variable width that occupy internal spaces with no clear pattern. Granellare strands yellowish-brown, branching, thread-like (width ~14 to 40 µm), in places attached to grain surfaces; barite crystals not observed.

**Etymology**

From the Latin '*contortus*', referring to the crooked and irregular appearance of different parts of the test.

**Material examined**

**Holotype**

NW PACIFIC OCEAN – **32.5° N (west of Kuroshio Extension Observatory (KEO))** • 32°34.81′ N, 143°46.24′ E; depth 5509 m; 22 Oct. 2022; H. Nomaki leg.; Dive 1659 of HOV *Shinkai 6500*, core Red#8; GenBank accession nos: PP662678, PP662679; National Museum of Nature and Science, Tsukuba, Japan, reg. no. TNS Pr695. The specimen is preserved in a core in 10% buffered formalin.

**Paratype**

NW PACIFIC OCEAN – **32.5° N (west of KEO)** • 1 spec.; same data as for holotype; Dive 1659 of HOV *Shinkai 6500*, core Red#7; National Museum of Nature and Science, Tsukuba, Japan, reg. no. TNS Pr694. The specimen is preserved in a core in 10% buffered formalin.

**Description**

**Overall test morphology**

*Holotype (TNS Pr695).* In the seabed photograph, the holotype (Fig. 2D) appears as an apparently unstructured cluster of plate-like elements of various shapes and sizes, including one that is fairly large and fan-shaped and others that are more elongate. Most of the main elements are orientated in the same general direction. Shipboard photographs (Supp. file 2: Fig. S4D) show a crooked, elongate, branched structure extending upwards with a small fan-shaped extremity, in addition to plate-like elements, most of which lean outwards away from the centre of the core.

The preserved specimen includes a main cluster of plate-like elements on one side, and on the other side, a smaller group of plates (not clearly visible in the seafloor image), part of which is attached to a stone (Supp. file 4: µCT video 2; Fig. 9A). A pebble-shaped xenophyophore, described below, partially separates these two groups. The overall appearance is confused and devoid of any obvious pattern. Many of the plates seem rather isolated, possibly because connections are obscured by resedimented material.

A μCT render showing the view from above reveals that the main cluster (length 59 mm, width 40 mm), at least, forms a single, complex, inter-connected structure lacking any obvious organisation (Fig. 9A). The other smaller group of plates (length 40 mm, width 15 mm) also seems to have some connection to the main cluster, although this is not entirely clear in the μCT render. The plates have complicated, irregular shapes and are either curved, sometimes strongly, or undulating (Fig. 9B–E; Supp. file 2: Fig. S5E–F; Supp. file 4: μCT video 2). In a few places they are punctuated by one or two small open spaces. The margins are typically lobate, and may give rise to more elongated, rounded, prong-like projections. Other crooked, elongate processes are also developed. The plates are about 1.0–1.7 mm (mean 1.33 ± 0.20 mm, n = 15) thick.

*Paratype (TNS Pr694)*. The in situ photograph shows a complex, confusing mass of irregular, poorly-resolved, and apparently plate-like elements, which is difficult to make sense of (Fig. 2C). Shadows suggest that some parts are upstanding. In the shipboard photograph, the most prominent part of the test is a large erect plate with vague concentric zones and an open space at its base (Supp. file 2: Fig. S4C). Adjacent to it is a recumbent plate that is curved into a trough-like structure, behind which two rounded lobes are visible. There is no sign of any symmetry or organisational pattern in either image.

By the time the paratype was examined in the shore-based lab, much of the test had collapsed. Some parts still projected upwards, but others that were originally upstanding lay flat on the surface of the preserved core (Fig. 10). These collapsed remnants measure 3.9 × 2.5 cm in maximum extent. The main features that remain in what appear to be their original positions are the trough-like plate, which is visible in the μCT renders and shipboard image, and the two rounded lobes (Fig. 10C–F; Supp. file 2: Fig. S5C–D), also seen in the shipboard photograph (Supp. file 2: Fig. S4C–D). These lobes arise from a plate that lies in a vertical plane; they are orientated more of less at right-angles to each other, one projecting vertically, the other horizontally. Some of the other structures visible in the light photographs and μCT scans probably represent parts of the large collapsed plate.

**Surface ornamentation, test structure and composition**

In light photographs, some of the plates display rather irregular concentric zones; these are most apparent on parts of the holotype (Fig. 9D–E) but also visible on the paratype (Fig. 10E; Supp. file 2: Fig. S5C). Radial features, however, have not been observed. Concentric zones with irregular boundaries can be seen in some μCT scans, which show that the internal space within the zones appears to be subdivided further into irregular spaces of different sizes and shapes (Fig. 9B). Micro-CT scans of the surface structure also reveal a rather faint pattern of shallow, cell-like depressions, some of them elongate, across parts of the test surface (Fig. 10B). These features are difficult to interpret. They cannot be seen in light photographs and whether they have any connection with the internal spaces is unclear.

The test wall is greyish, friable, 210–340 μm (mean 295 ± 0.04 μm, n = 15) thick and similar to that of *Psammina yokosukae* sp. nov. When viewed through the wall of the core tube, the test surface in areas not covered in redeposited sediment includes a scattering of larger grains (Supp. file 2: Fig. S5C). Seen under a stereo microscope, the wall is composed of mineral grains of various sizes (Fig. 5A–C). The larger grains are often dark, with a smaller proportion that are whitish and orange.

**Stercomare and granellare**

The stercomare resembles that of *Psammina yokosukae* sp. nov. in consisting of branches and more irregular masses with varying dimensions that occupy spaces between internal particles and do not conform to any particular trend or pattern. Similarly, the granellare forms narrow strings with a width of 14–40 μm (usually 20–30 μm, mean 24.8 ± 7.26 μm, n = 46). They are closely associated with the internal agglutinated particles and in places are attached to them. The granellare was not observed using SEM, but a strand examined using transmitted light under a high-power microscope did not contain any obvious barite crystals (Fig. 8F–G).

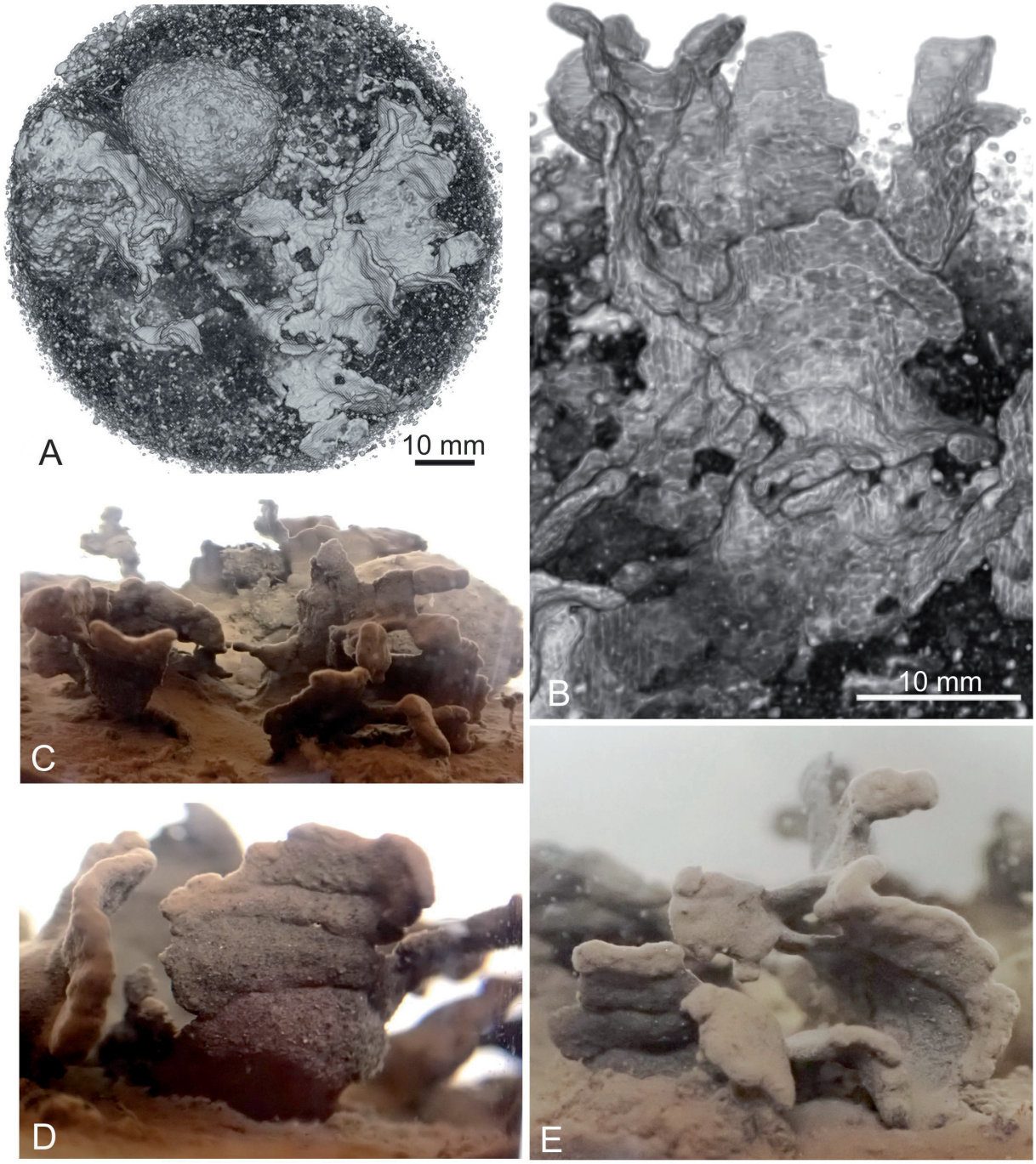


**Fig. 9.** *Psammina contorta* sp. nov., holotype, reg. no. TNS Pr695. **A**. Micro-CT render showing exterior surface of complete test, as seen from above; the rounded object is the 'pebble-shaped, honeycombed xenophyophore' (TNS Pr696) informally described below. **B**. Micro-CT render showing interior features of part of the test, viewed obliquely; note the apparent compartmentalization of the test interior. Note that both images include parallel stripes that are obviously artifacts. **C–E**. Light photographs of parts of the test seen through the curved wall of the core tube, which causes some optical distortion.

**Molecular characterisation**

*Psammina contorta* sp. nov. is strongly supported by the BV (98%) and branches at the base of *P. tenuis* and *P. yokosukae* sp. nov. The group is supported by 99% BV. The sequenced 18S barcoding fragment of *P. contorta* sp. nov. contains 1036 nucleotides and the GC content is 36%. The obtained sequences are identical.

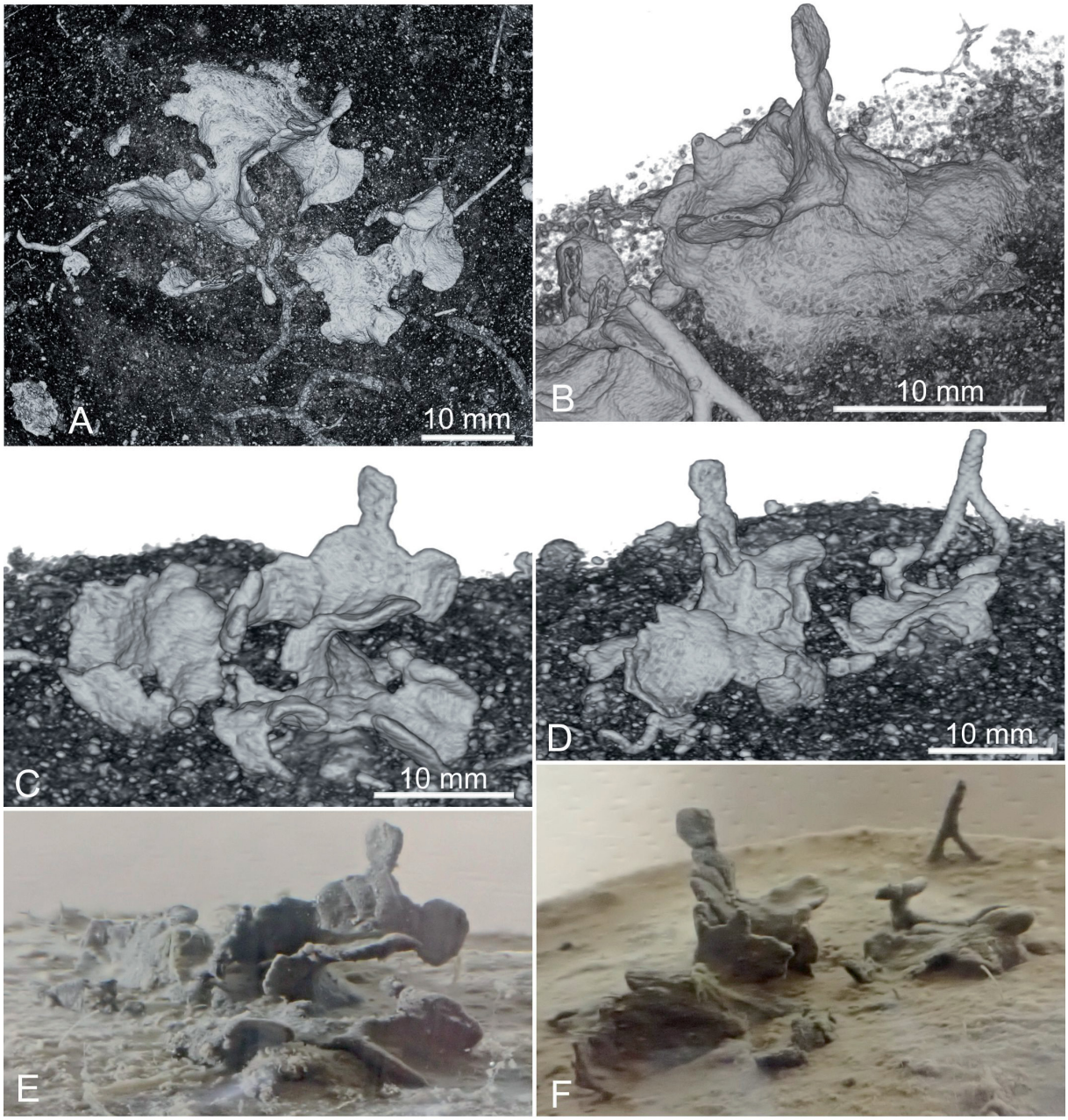


**Fig. 10.** *Psammina contorta* sp. nov. paratype, reg. no. TNS Pr694. **A–D**. Micro-CT renders showing exterior surface of test. **A**. Complete test as seen from above. **B**. Oblique view of part of the test; note the cell-like pattern on the surface. **C–D**. Slightly oblique side views of the complete test. **E–F**. Light photographs of views similar to those shown in C–D, as seen through the curved wall of the core tube, which causes some optical distortion.

**Remarks**

*Psammina contorta* sp. nov. resembles *P. yokosukae* sp. nov. in many respects, notably the test structure, the size and composition of the agglutinated grains, and the organisation of the stercomare and granellare systems. However, there are two main morphological differences. First, the test of *P. contorta* is a highly irregular structure made up of plates of various sizes and shapes that appear somewhat disconnected, in contrast to the more coherent system of fairly well-formed branching plates that characterise the holotype of *P. yokosukae*. Second, although concentric zones are visible in both light photographs and μCT scans of *P. contorta*, there is no evidence for internal radial structures running between the zones. Instead, μCT renders appear to show the interior occupied by the irregularly shaped spaces. These rather different morphological characteristics, together with the genetic data, support the recognition of two distinct species.

As in the case of *Psammina yokosukae* sp. nov., our phylogenetic reconstruction shows that *P. contorta* sp. nov. is a close relative of *P. tenuis* and has similarly narrow granellare branches that are, to some extent, attached to internal test particles. Moreover, the disorganised test is morphologically quite different from the simple curved plate of *P. tenuis*. As also noted above for *P. yokosukae*, a particularly striking difference is that the test of *P. tenuis* is composed largely of radiolarian tests, whereas that of *P. contorta* consists of mineral grains.

Genus ***Laminarena*** gen. nov.
urn:lsid:zoobank.org:act:0B9D4CF3-8CC3-49B1-85BB-966EFBBD7C4A

**Type species**

*Laminarena variabilis* gen. et sp. nov. described below.

**Diagnosis**

Test free, epifaunal, up to at least 6.3 cm maximum dimension. Comprising several thin, delicate, curved or undulating plates with sinuous margins and occasional branches, typically arranged asymmetrically. Obvious apertures absent. Plates marked by concentric zones, traversed by low, closely spaced, radial ridges, together forming distinctive surface ornamentation. Plate walls composed of mineral grains including larger dark particles set in lighter-coloured, fine-grained matrix. Test interior without internal particles except for partitions corresponding to external radial ridges. Dark stercomare branches and pale granellare strands (width 45–100 μm) follow same radial trend. Granellare containing numerous barite crystals.

**Etymology**

A combination of the Latin words '*laminam*' ('plate') and '*arena*' ('sand'), referring to the basically plate-like agglutinated test. Gender feminine.

**Remarks**

Phylogenetically, *Laminarena* gen. nov. is close to the genus *Aschemonella* Brady, 1879, grouping together with *A. aspera* Gooday & Holzmann, 2017 and *Aschemonella* sp. 3 sensu Gooday *et al.* (2017b). However, the two genera have little in common morphologically, apart from the fact that the test is agglutinated and internal xenophyae absent. The new genus is characterised by a basically plate-like test, whereas in *Aschemonella*, the test is either a tube interrupted by internal partitions or a sequence of more or less globular chambers. Given these striking morphological differences, we feel justified in establishing this new genus.

***Laminarena variabilis*** gen. et sp. nov.
urn: lsid:zoobank.org:act:A7159F47-DD82-4C93-A3A4-D26481268FF2
Figs 11–19, 21A–E, 22A; Supp. file 2: Figs S6–S14; Supp. files 5, 6; µCT videos 3–4

'*Xenophyophores*' – Tsuchiya & Nomaki 2021: figs 1–3.

**Diagnosis**

As for genus.

**Etymology**

Latin, '*variō*' ('diverse or variable') + suffix '*-bilis*', adjective, referring to the variable morphology.

**Material examined**

**Holotype**

NW PACIFIC OCEAN – **30° N** • 30°09.2′ N, 143°35.1′ E; depth 5366 m; 23 Oct. 2022; H. Nomaki leg.; Dive 1660 of HOV *Shinkai 6500*, core Blue#2; GenBank accession no.: PP662670; National Museum of Nature and Science, Tsukuba, Japan, reg. no. TNS Pr700. The specimen is preserved in a core in 10% buffered formalin.

**Paratype**

NW PACIFIC OCEAN – **30° N** • 1 spec.; same data as for holotype; Dive 1660 of HOV *Shinkai 6500*, core Blue#1; National Museum of Nature and Science, Tsukuba, Japan, reg. no. TNS Pr699. The specimen is preserved in a core in 10% buffered formalin.

**Other material examined**

NW PACIFIC OCEAN – **30° N** • 1 spec.; same data as for holotype; Dive 1660 of HOV *Shinkai 6500*, core Blue#6; National Museum of Nature and Science, Tsukuba, Japan, reg. no. TNS Pr702 • 1 spec.; same data as for holotype; Dive 1660 of HOV *Shinkai 6500*, core Blue#7; National Museum of Nature and Science, Tsukuba, Japan, reg. no. TNS Pr703 • 1 spec.; same data as for holotype; Dive 1660 of HOV *Shinkai 6500*, core Red#4; National Museum of Nature and Science, Tsukuba, Japan, reg. no. TNS Pr705. – **32.5 °N** • 1 spec.; 32°34.8′ N, 143°46.2′ E, depth 5505 m; 22 Oct. 2022; H. Nomaki leg.; Dive 1659 of HOV *Shinkai 6500*, core Red#9; National Museum of Nature and Science, Tsukuba, Japan, reg. no. TNS Pr697 • 1 spec.; 32°34.7′ N, 143°46.1′ E; depth 5505 m; 24 May 2022; H. Nomaki leg.; Dive 1633 of HOV *Shinkai 6500*, core Blue#1; National Museum of Nature and Science, Tsukuba, Japan, reg. no. TNS Pr690 • 1 spec.; 32°34.9′ N, 143°45.9′ E; depth 5505 m; 27 May 2023; H. Nomaki leg.; Dive 1691 of HOV *Shinkai 6500*, core Blue#0; National Museum of Nature and Science, Tsukuba, Japan, reg. no. TNS Pr714. Specimens are preserved in cores in 10% buffered formalin.

**Description of the typical 30° N form**

**Overall test morphology**

The test comprises a more or less complex, asymmetrical system of thin, interconnected plates that follow a curved, or undulating course. Although the plates may appear to some extent separate, in fact they are either parts of one longer, highly sinuous plate or linked to other plates at branching points. There is considerable variation in test morphology and each specimen is different. Micro-µCT scans show that the tests do not penetrate the sediment to any extent and there is no evidence for root-like structures.

*Holotype (TNS Pr700)*. The seabed photograph of the holotype (Supp. file 2: Fig. S6A) shows two relatively simple, curved plates with the concave sides facing outwards, and another more complex branching plate, all of them displaying concentric zones. In µCT renders, the recovered specimen

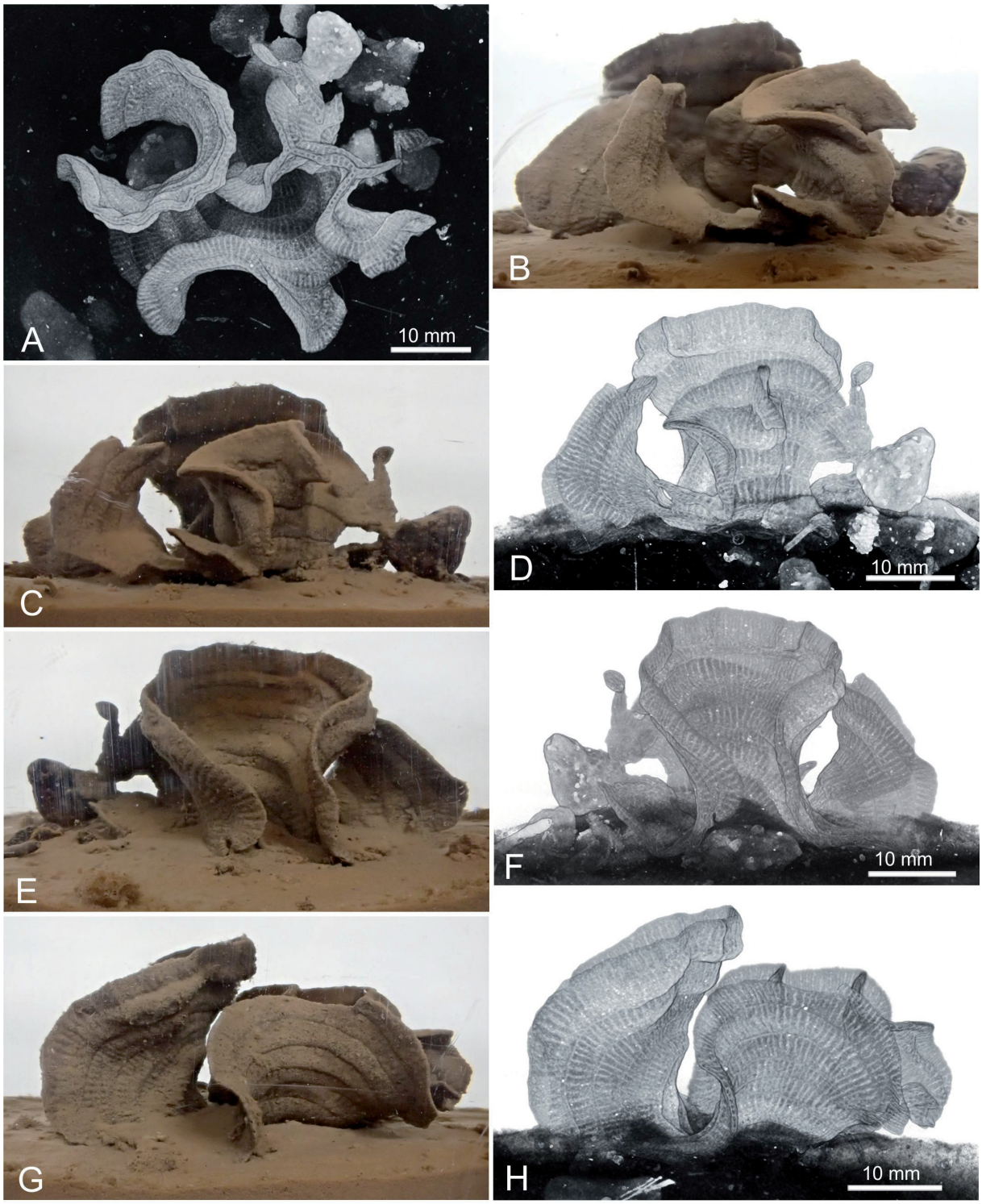


**Fig. 11.** *Laminarena variabilis* gen. et sp. nov., typical 30° N form, holotype, reg. no. TNS Pr700. **A**. Micro-CT render showing internal features of complete test, as seen from above. **B**. Light photograph showing side view of test as seen in through the core tube wall. **C–H**. Light photographs and corresponding µCT renders showing different side views of test. The light photographs are somewhat distorted as a result of being photographed through the curved core-tube wall, whereas the µCT renders show the true shape.

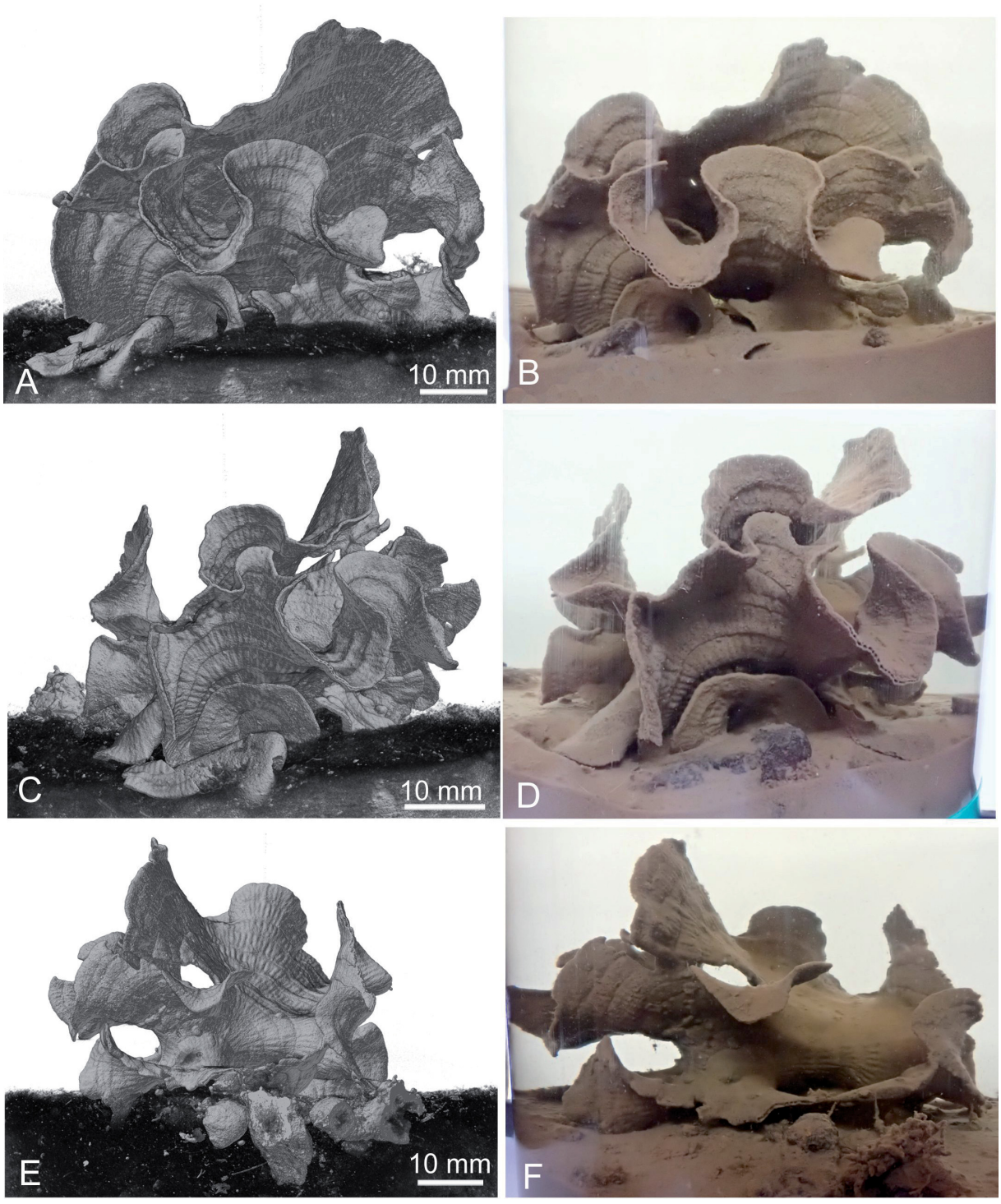


**Fig. 12.** *Laminarena variabilis* gen. et sp. nov., paratype, typical 30° N form, reg. no. TNS Pr699. Micro-CT renders showing exterior surface of test from different angles, and corresponding light photographs taken through the curved wall of the core tube. Note that the light photographs are somewhat distorted whereas the μCT renders show the true shape of the test.

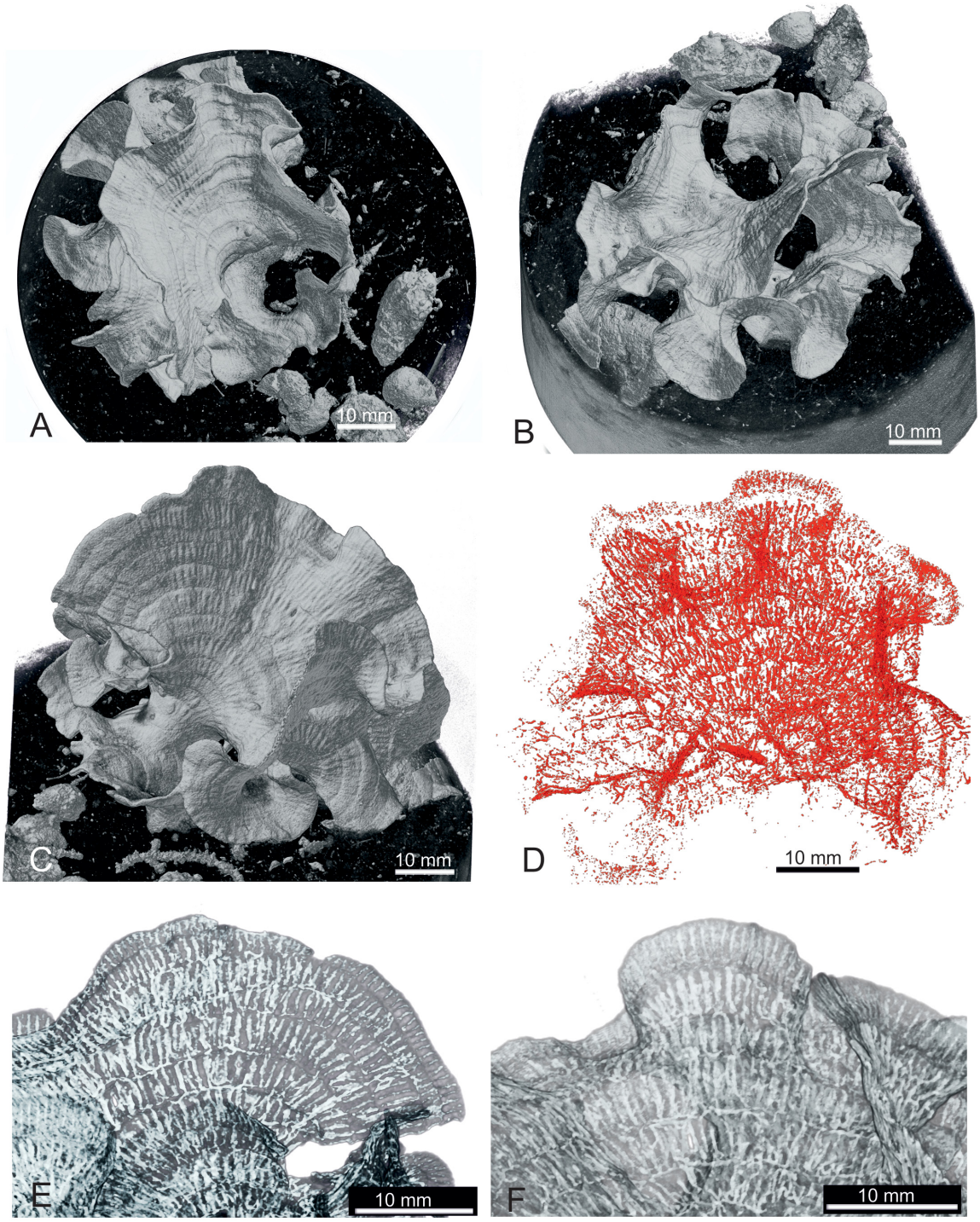


**Fig. 13.** *Laminarena variabilis* gen. et sp. nov., typical 30° N form, paratype, reg. no. TNS Pr699. **A–C**. Micro-CT renders showing exterior surface of test; note surface expression of internal structure. **A**. View from directly above. **B**. Oblique top view showing the other side of the test. **C**. Oblique side view. **D**. 3D μCT reconstruction of X-ray dense internal features interpreted as granellare strands filled with barite crystals; orientation of the specimens was similar to that shown in Fig. C. **E–F**. Micro-CT renders showing details of the test interior. The white roughly linear, radial structures are interpreted as granellare strands; note also, particularly in Fig. F, the presence of some strands running horizontally, parallel to the base of the concentric zones.

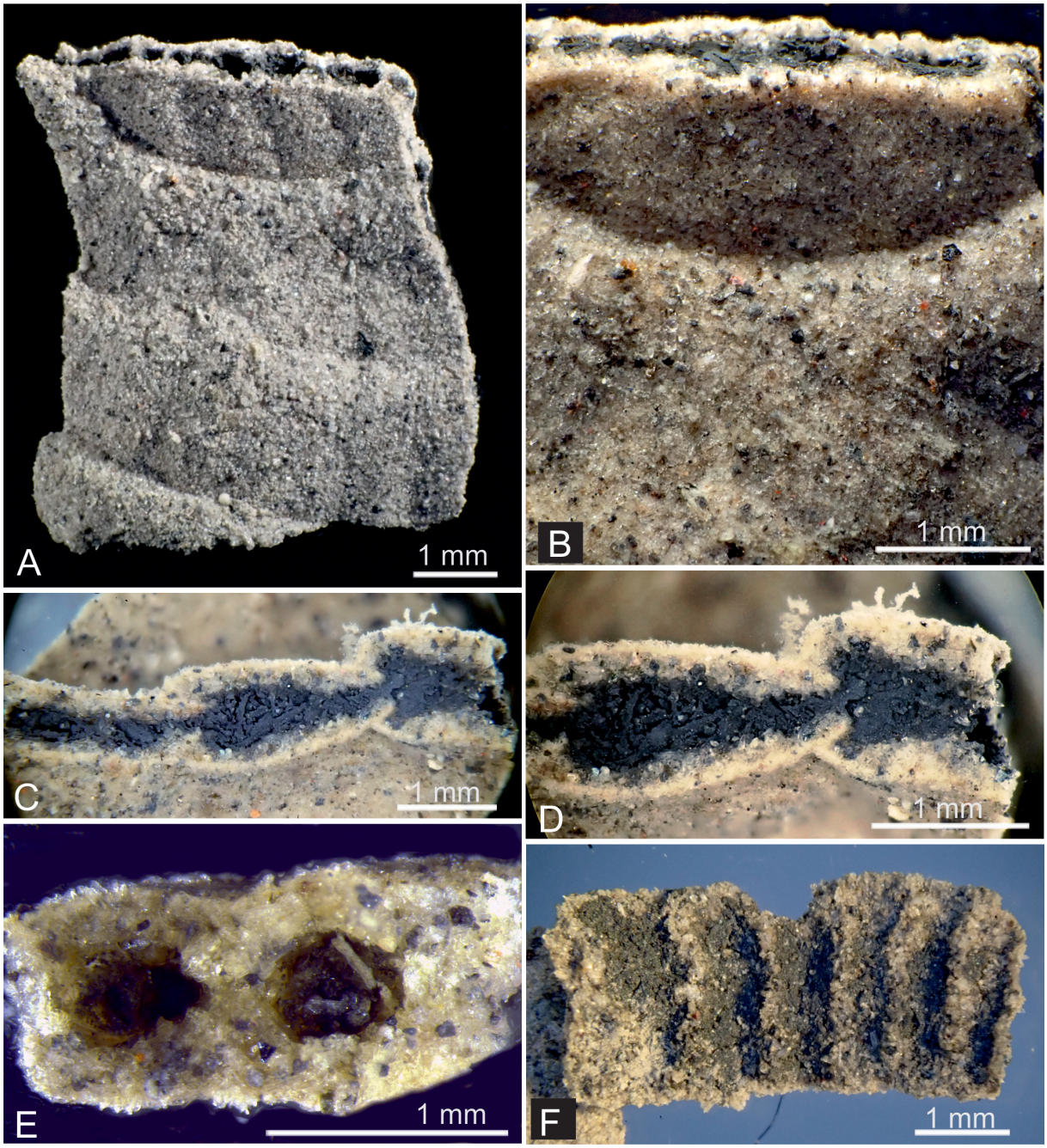


**Fig. 14.** *Laminarena variabilis* gen. et sp. nov., typical 30° N form, stereo microscope photographs of fragments of two additional specimens. **A–D**. Additional specimen reg. no. TNS Pr705. **A**. Fragment of test showing parts of several concentric zones, one of them with low radial ridges. The direction of growth is from top to bottom. **B**. Detail of boundary between two concentric zones. **C–D**. Broken cross sections across concentric zones; note the overlap between successive zones. The direction of growth is from left to right. **E–F**. Additional specimen reg. no. TNS Pr702. **E**. Broken section across radial features showing internal partitions. **F**. Internal surface of test wall showing partitions.

measures 49 mm by 39 mm in maximum extent and projects to a height of 24 mm above the sediment surface (Fig. 11A, D, F, H). The view from above shows the three main plate-like components that are visible in the seafloor image (Fig. 11A). The plates are thin and delicate, ranging in thickness from 1.2–1.5 mm (mean 1.35 ± 0.12 mm, n = 15). They appear somewhat separated but the μCT video (Supp. file 5) shows that all three arise from a common basal area. Two are relatively simple plates facing at approximately 90 degrees to each other. The largest is strongly curved and forms an almost complete circuit, the second less strongly curved. The third main element branches to create a more

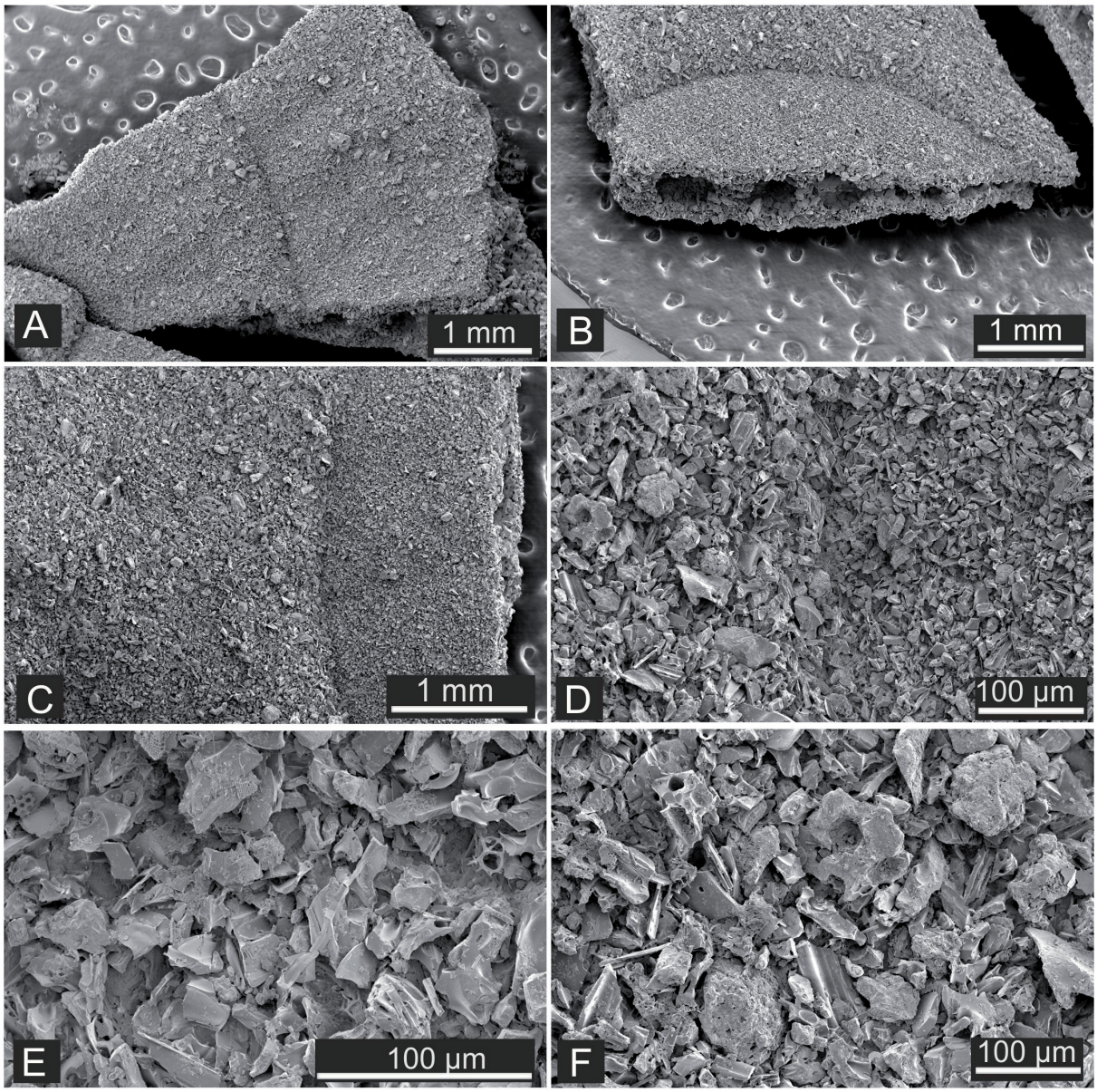


**Fig. 15.** *Laminarena variabilis* gen. et sp. nov., typical 30° N form, SEM images (secondary electron mode) of two fragments of additional specimen reg. no. TNS Pr705. **A**. First fragment. **B**. Second fragment. **C–D**. Details of the second fragment showing boundary between concentric zones (direction of growth from right to left); note the increase in grain size of the agglutinated particles at the base of the new zone. **E**. Detail of agglutinated surface of the younger zone. **F**. Detail of agglutinated surface of the older zone.

complex undulating structure with a sinuous upper margin when viewed from above (Fig. 11A). One part is attached for a short distance to a stone (Fig. 11C–F) and Supp. file 5 appears to show that the largest plate is also attached to a stone. It is possible that the part of the test immediately adjacent the former stone represents the base from which the rest of the test developed.

*Paratype (TNS Pr699)*. The seabed image (Supp. file 2: Fig. S6B) is dominated by a large, unevenly curved plate with the concave side facing outwards, behind which several additional sinuously curved plates are visible. The recovered specimen is contained within a roughly hemispherical envelope. In µCT renders (Figs 12A, C, E, 13A–C) it measures 63 mm by 58 mm in maximum extent and projects to a height of 42 mm above the sediment surface, making it the largest of the six specimens. The plates range in thickness from 0.60 to 0.85 mm (mean 0.72 ± 0.09 mm, n = 13). The test appears to lie directly on the sediment surface with no obvious structures penetrating the sediment (Supp. file 6: µCT video 4). The view from directly above (Fig. 13A) reveals a strongly asymmetrical morphology. The plates are located mainly on one side of an open space through which the sediment is visible, with the largest plate dominating the view and partly obscuring the rest of the test. Other µCT renders and light images

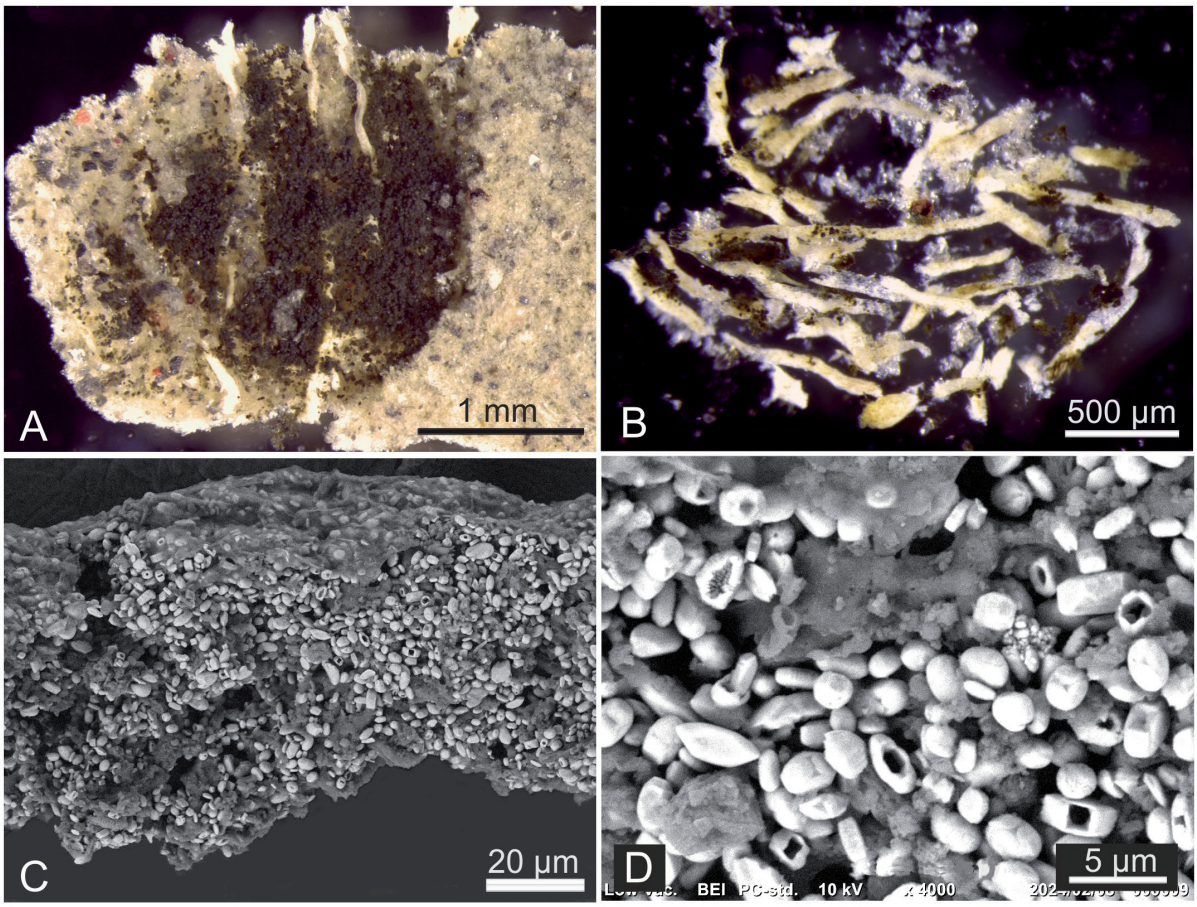


**Fig. 16.** *Laminarena variabilis* gen. et sp. nov., typical 30° N form, paratype, reg. no. TNS Pr699. **A–B**. Stereo microscope images. **A**. Test interior showing damaged stercomare and granellare strands running between the internal partitions. **B**. Granellare strands dissected for genetic analysis. **C–D**. SEM images (low vacuum, backscatter mode) of granellare strand. **C**. Overview to show large numbers of barite crystals, clearly seen where the granellare tube has disintergrated; remnants of the flimsy tube remain in places. **D**. Detail of crystals; note that some are interrupted by deep, sometimes rectangular, depressions. A–B taken in Geneva.

(Figs 12, 13B–C) show a series of smaller, often strongly curved plates with sinuous rims. Several small, curved plates near the base of the test form tunnel-like features at or just above the sediment surface. There are no reticulations, although the video (Supp. file 6) clearly shows several points at which the plates branch (see also Fig. 12A, C–D). It is also clear from the video that large sections of the test, including the largest plate and others that appear separate from it in some views, in fact comprise a single continuous and highly sinuous plate (Fig. 13B).

The test has no current connection with several small stones that lie nearby in the core (Fig. 13A). However, careful examination of the μCT renders (Fig. 13A) suggests that a short broken section of the margin near the base of the largest plate was probably originally attached to one of the stones, which still retains a small fragment of the plate on its surface. As in the holotype, it seems likely that this region near the base of the largest plate represents the initial part of the test.

*Additional specimen reg. no. TNS Pr705*. In μCT scans the specimen measures 50 mm by 48 mm in maximum extent and projects to a height of 40 mm above the sediment surface. The seafloor image (Supp. file 2: Fig. S6C), together with laboratory photographs and μCT renders (Supp. file 2: Fig. S7), all show what appears to be one continuous main plate that makes several sinuous, sweeping loops in different planes. The largest loop is directed vertically, creating a broad, funnel-like structure that opens in an upward direction, while in the lower part of the test the loops are orientated horizontally (see particularly Supp. file 2: Fig. S7A, E). There are also several additional curved plates near the base of the structure that possibly arise as branches of the main plate, although obvious branching points cannot be seen.

*Additional specimen reg. no. TNS Pr702*. The test appears simpler than others in seafloor images. A strongly curved upper plate creates a funnel-like structure through which the sediment surface is visible (Supp. file 2: Fig. S6D). At least one additional plate can be seen beneath the upper plate. The recovered specimen is located to one side of the core and seems to have slumped slightly. It measures 51 mm by 50 mm in maximum extent, projects to a height of 44 mm, and has a distinctly asymmetrical appearance. The μCT top view render shows two strongly concave plates that face in different directions but are linked together to create a single large plate with a strongly sinuous, S-shaped margin (Supp. file 2: Fig. S8A). In side view, another large plate that is strongly curved on a horizontal plane appears to be continuous with the sinuous upper plate (Supp. file 2: Fig. S8B). On one side it branches to give rise to a smaller plate that is curved in the same direction and at one point is attached to a stone (Supp. file 2: Fig. S8B–D). Both these elements merge together into a gently undulating plate near the base of the test.

*Additional specimen reg. no. TNS Pr703*. In the seafloor and shipboard images this large specimen is clearly more complex than others and gives the impression of being made up of a larger number of smaller plates (Supp. file 2: Fig. S6E–F). The recovered specimen measures 60 mm by 55 mm in maximum extent and projects to a height of 35 mm. As in the shipboard image, the test appears to comprise numerous curved plates that are orientated in different directions, but with no clear pattern or obvious reticulations (Supp. file 2: Fig. S9). These elements are all interconnected and it is clear from Supp. file 2: Fig. S9A (top view), that many plates that appear distinct from some angles are actually parts of at least two larger plates. One of these is sinuously folded into an S shape, the other follows a straighter course. In places, the plates clearly branch or give rise to side plates. Many parts of the plate system extend upwards but near the base of the test some are more horizontal with their concave sides facing downwards.

**Surface ornamentation, test structure and composition**

The test surfaces of all specimens display a distinctive pattern of concentric zones that follow the shape of the plate margin and are traversed at right angles by low radial ridges separated by shallow

furrows (Figs 12, 14A). These features create a distinctive pattern that in places is strongly developed (Supp. file 2: Fig. S7F). In the holotype, the zones are 1.8–5.6 mm (mean 3.23 ± 1.28 mm, n = 7) wide and the radial ridges spaced 0.46–0.70 mm (mean 0.57 ± 0.07 mm, n = 14) apart. In the paratype, the zones also measure between 1.8 and 5.6 mm (usually 2.3–3.9 mm; mean 3.11 ± 0.84 mm, n = 21) wide and the radial ridges are spaced 0.46–0.74 mm (mean 0.57 ± 0.08 mm, n = 16) apart. One of the plates of additional specimen TNS Pr703 features a number of dome-like surface pustules that can be seen in the μCT render (Supp. file 2: Fig. S9B).

The test plates are 250–320 μm (mean 0.28 ± 0.02 μm, n = 16) thick and comprise two more or less parallel walls. Sections that have broken across the concentric zones (i.e., at right angles to the test margin) show that the walls of later (younger) zones overlap those of the preceding zones (Fig. 14C–D), rather than being a simple continuation of the wall. Sections of the test that have broken across the radial ridges (i.e., parallel to the concentric zones and to the test margin) often show that the interior is interrupted by transverse partitions that define compartments (Fig. 14E). Micro-CT scans (Figs 11–13; Supp. file 2: Figs S7–S9) confirm that the surface pattern of radial ridges and furrows corresponds to these internal partitions. When test fragments are broken to expose the interior, the partitions can be seen as low, parallel structures composed of agglutinated particles arising from the inner surface of the wall (Fig. 14F). Otherwise, the test interior appears largely devoid of internal particles.

The wall is greyish in overall colour when dried and composed of a mixture of mineral grains of varying sizes (Figs 14A–B, 15). Most of the larger particles are dark but a few are transparent or whitish, although the density of darker grains is higher in some fragments than in others. SEM images show a jumble of particles, mainly of mineral origin and many resembling fragments of volcanic glass (Fig. 15E–F). There is also a tendency for the grain size to increase from the inner to the outer part of a zone (Fig. 15A–C), thereby creating a contrast in grain size across zone boundaries (Fig. 15C–D).

**Granellare and stercomare**

The granellare strands are generally located between the internal partitions (Fig. 16A). They are whitish to pale yellow, branch occasionally, and 45–97 μm wide (mean 67.4 ± 12.8 μm, n = 34). In the fragments examined, the spaces between the partitions are also occupied by masses of loose stercomata or their degraded remnants. In μCT scans of the paratype, the granellare strands appear as bright threads that correspond to the radial lineations (Fig. 13E–F). They are present throughout much of the test but less well developed near the base and more strongly developed towards one side of the upper part (Fig. 13D). The threads branch to some extent. In places near the margin, they appear to be discontinuous across the boundary between the two outer concentric zones (Fig. 13F). In addition to the main radial trend of the granellare, strands running horizontally are visible near the base of some of the concentric zones. Viewed by SEM, fragments of granellare are packed with crystals, a few microns (<5 μm) in size and identical to the barite particles ('granellae') that are typical of xenophyophores (Fig. 16C–D). Some crystals are marked by deep, sometimes rectangular depressions.

**Description of 32.5° N form**

This form is represented by two specimens from which we obtained molecular sequences, one collected in 2022 during dive 1659 (TNS Pr697) and the other in 2023 during dive 1691 (TNS Pr714). A third morphologically similar specimen was collected in 2022 during dive 1633 (TNS Pr690) but was immediately preserved in formalin and could not be sequenced.

**Overall test morphology**

*Specimen reg. no. TNS Pr697.* The test comprises a complex system of irregularly shaped but generally plate-like elements that are often somewhat curved (Fig. 17A–F; Supp. file 2: Fig. S10A–B). In μCT scans, the specimen has an overall extent of ~4.3 cm and rises ~1.8 cm above the sediment surface. The

central part seems to be generally flat lying, but around the periphery, a series of complicated, elongate elements, some of which branch, project upwards to varying extents and at various angles. Four or five of these elements are particularly conspicuous. They project mainly to one side, giving the test an asymmetrical appearance, and tend to widen upwards, sometimes with a vaguely fan-like termination. The plates range in thickness from 0.9 to 1.3 mm (mean 1.08 ± 0.12 mm, n = 15) and are punctuated by a few open spaces. One section of the periphery forms an undulating margin that rises only slightly from the surface. Concentric zones can be seen across many parts of the test surface (Fig. 17F).

*Specimen reg. no. TNS Pr714*. This specimen is similar in overall appearance to TNS Pr697. It forms a delicate structure that includes several fan-shaped plates, one of which is larger than the others (Fig. 17G; Supp. file 2: Figs S10D, S11). The larger plate is connected to two smaller plates; and one of these merges with a fourth plate that develops from a separate stem. This cluster of plates is linked, in turn, to an irregular formation that includes several bar-like components and irregular excrescences; this part cannot be seen clearly through the core tube because it lies on the edge of the core and is partly obscured by redeposited sediment. The largest plate displays concentric zones and indistinct radial ridges (Fig. 17H), features that are clearly evident in the fragment illustrated in Fig. 18C.

*Specimen reg. no. TNS Pr690*. The seabed photograph shows a compact cluster of irregular elements, some of them plate-like (Supp. file 2: Fig. S10E). In the shipboard photograph, the largest element terminates in a distinct fan, punctuated by two elongate open spaces, while bar-like structures project out to one side (Supp. file 2: Fig. S10F). In the µCT render showing the top view, the test appears as a chaotic jumble of relatively small, irregular plate-like elements (Supp. file 2: Fig. S12A). It measures 6.1 cm by 5.9 cm in maximum extent and projects 3.1 cm above the sediment surface. The test structure is clearer in side view renders that show a number of elongate processes that widen to varying extents towards their extremities (Supp. file 2: Fig. S12B–C). These include the fan visible in the shipboard photograph. This and many of the other test parts are orientated upwards at an angle of 40° or more, and are clustered around a prominent, straight, chimney-like tube. However, there are also some narrow structures near the base of the test that extend outwards at a lower angle. In a few places, the plates are perforated by open spaces. The chimney-like tube is probably that of a polychaete. In the shipboard photograph, the upper part of this tube is obscured by a mass of detritus (Supp. file 2: Fig. S10F).

**Surface ornamentation, test structure and composition.**

Although the surface ornamentation that is a feature of the 30° N specimens is less evident in the 32.5° N form, corresponding internal features are obvious in the µCT images of specimen TNS Pr697 (Fig. 17B–C) and particularly specimen TNS Pr690 (Supp. file 2: Fig. S12B–E). These show a distinct pattern of concentric zones and radial structures, presumably internal partitions. The zones are 1.5–4.1 mm (mean 2.88 ± 0.81 mm) wide and the radial features spaced 0.50–1.22 mm (mean 0.87 ± 0.19 mm, n = 17) apart. Partitions are seen in broken cross sections of the specimen TNS Pr714 fragment viewed under a stereo microscope but their development is variable, ranging from vaguely defined to well defined (Fig. 18D–E). Partitions appeared weakly developed on inner test surfaces when this fragment was broken open and viewed under a light microscope (Fig. 18F–G) but were rather more obvious in an SEM image (Fig. 19A).

In specimens TNS Pr697 and particularly Pr714, the test wall resembles that of the holotype and paratype (Fig. 18A–C; Supp. file 2: Fig. S13A). It is composed of mineral particles of varying sizes, with a matrix of small grains intermingled with a subordinate number of larger grains, mainly whitish and black but occasionally orange. Many of the whitish ones are probably volcanic glass (Supp. file 2: Fig. S13B). The largest are a few hundred microns in size but most are much smaller.

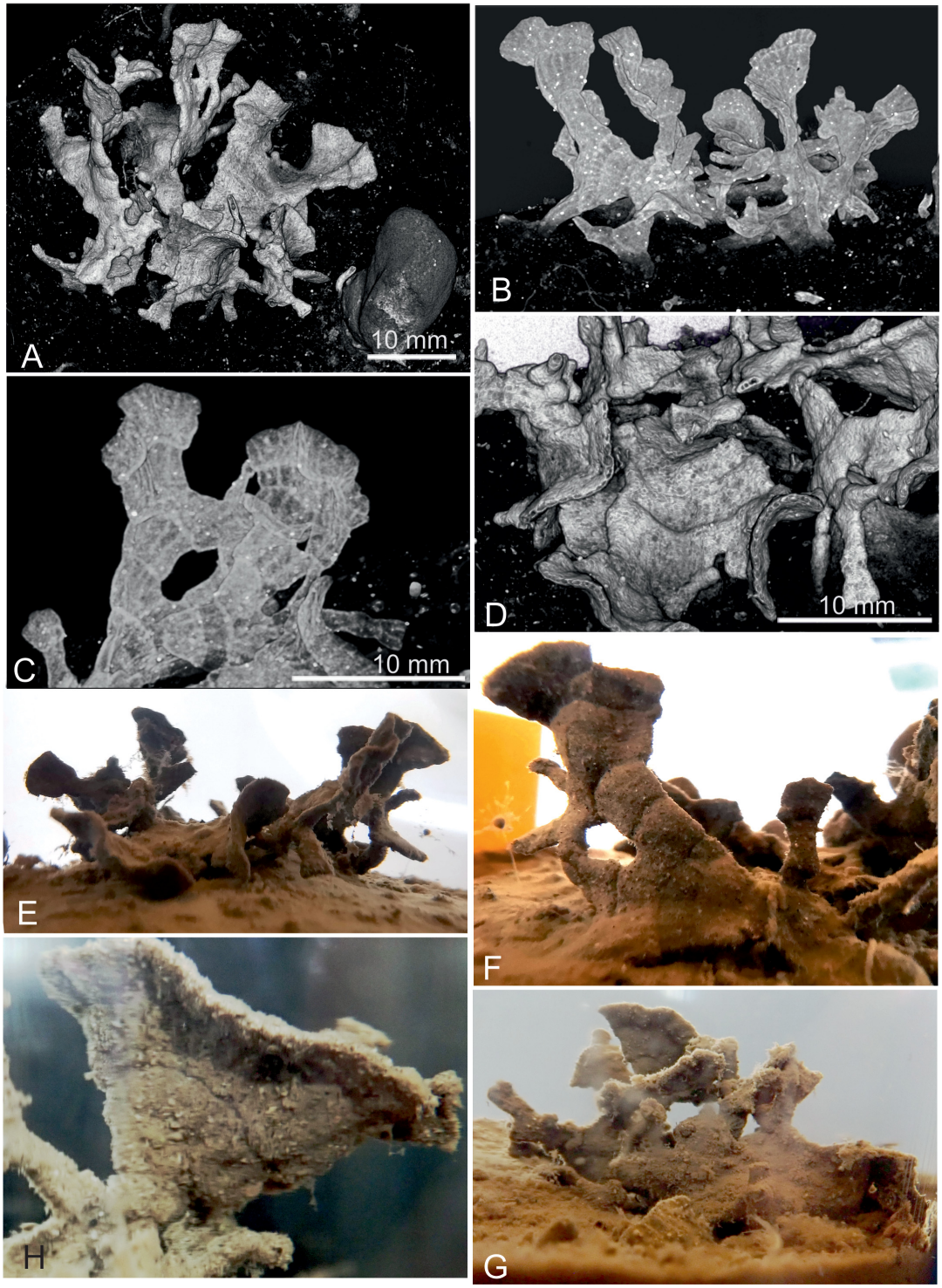


**Fig. 17.** *Laminarena variabilis* gen. et sp. nov., 32.5° N form. **A–F**. Specimen reg. no. TNS Pr697. **A–D**. Micro-CT renders. **A**. Oblique view of test from above showing surface features. **B**. Side view showing internal features. **C**. Detail of internal features of text extremities. **D**. Detail of test surface. **E–F**. Light photographs showing side views of test as seen through the core tube wall. **E**. Complete test. **F**. Detail showing concentric zones. **G–H**. Specimen reg. no. TNS Pr714. **G**. Complete specimen. **H**. Large fan-shaped extremity showing concentric zones and radial ridges. Note that the light photographs are somewhat distorted by the curvature of the tube wall.

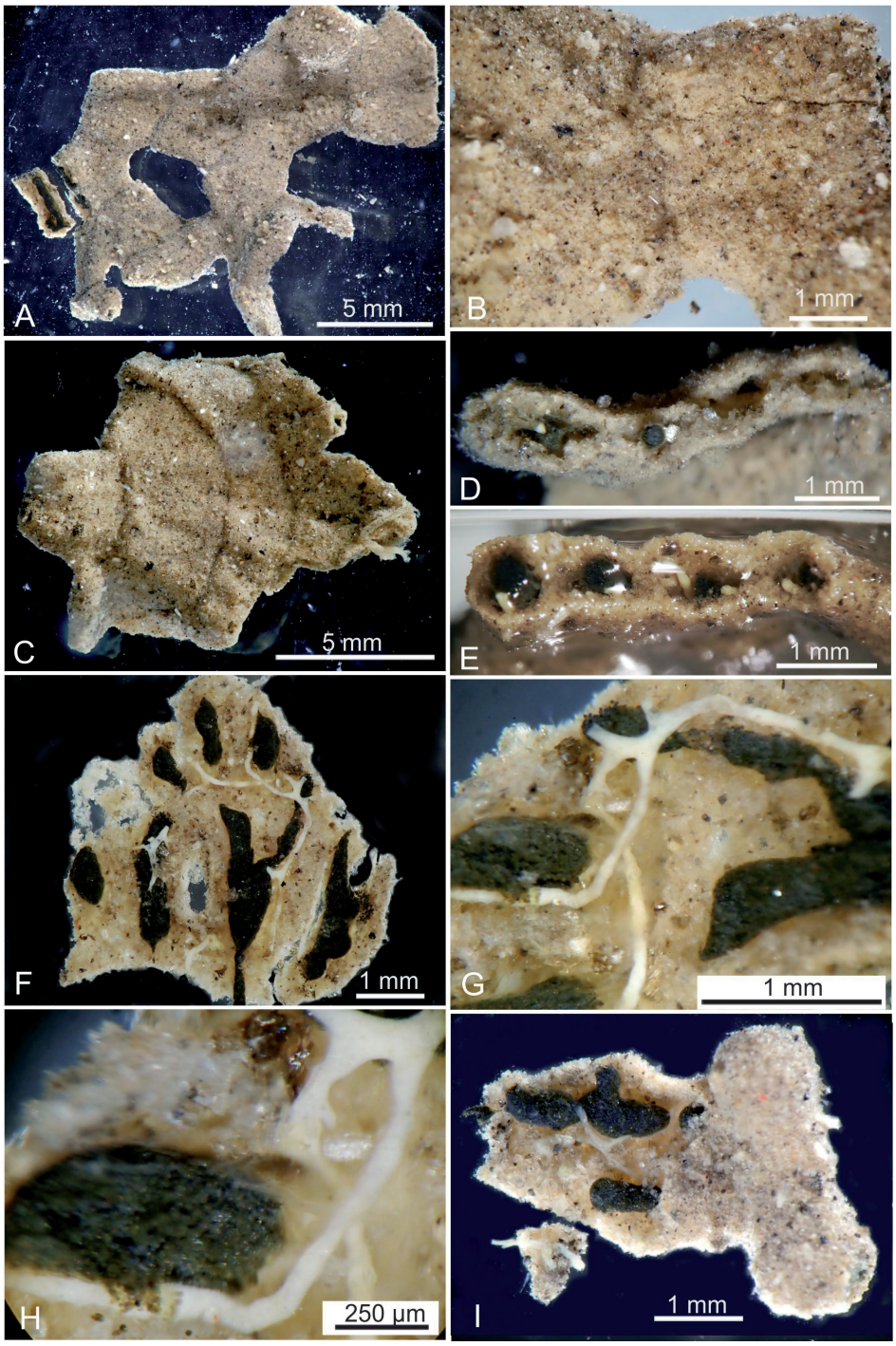


**Fig. 18.** *Laminarena variabilis* gen. et sp. nov., 32.5° N form; stereo microscope images. **A–B**. Specimen reg. no. TNS Pr697. **A**. Entire fragment; this is the same part of the test as that illustrated in Fig. 17B. **B**. Detail of test surface. **C–H**. Specimen reg. no. TNS Pr714. **C**. Entire fragment showing concentric zones and low radial ridges. **D**. Broken edge of fragment with poorly developed partitions. **E**. Another broken edge of the same fragment with clearly developed partitions. **F**. Fragment broken open to show dark stercomare and pale granellare strands. **G**. Detail of granellare and stercomare. **H**. Detail showing stercomare and granellare in close proximity. **I**. Fragment of specimen reg. no. TNS Pr697 broken open to show stercomare and granellare, similar to those of specimen TNS Pr714. All images taken at JAMSTEC.

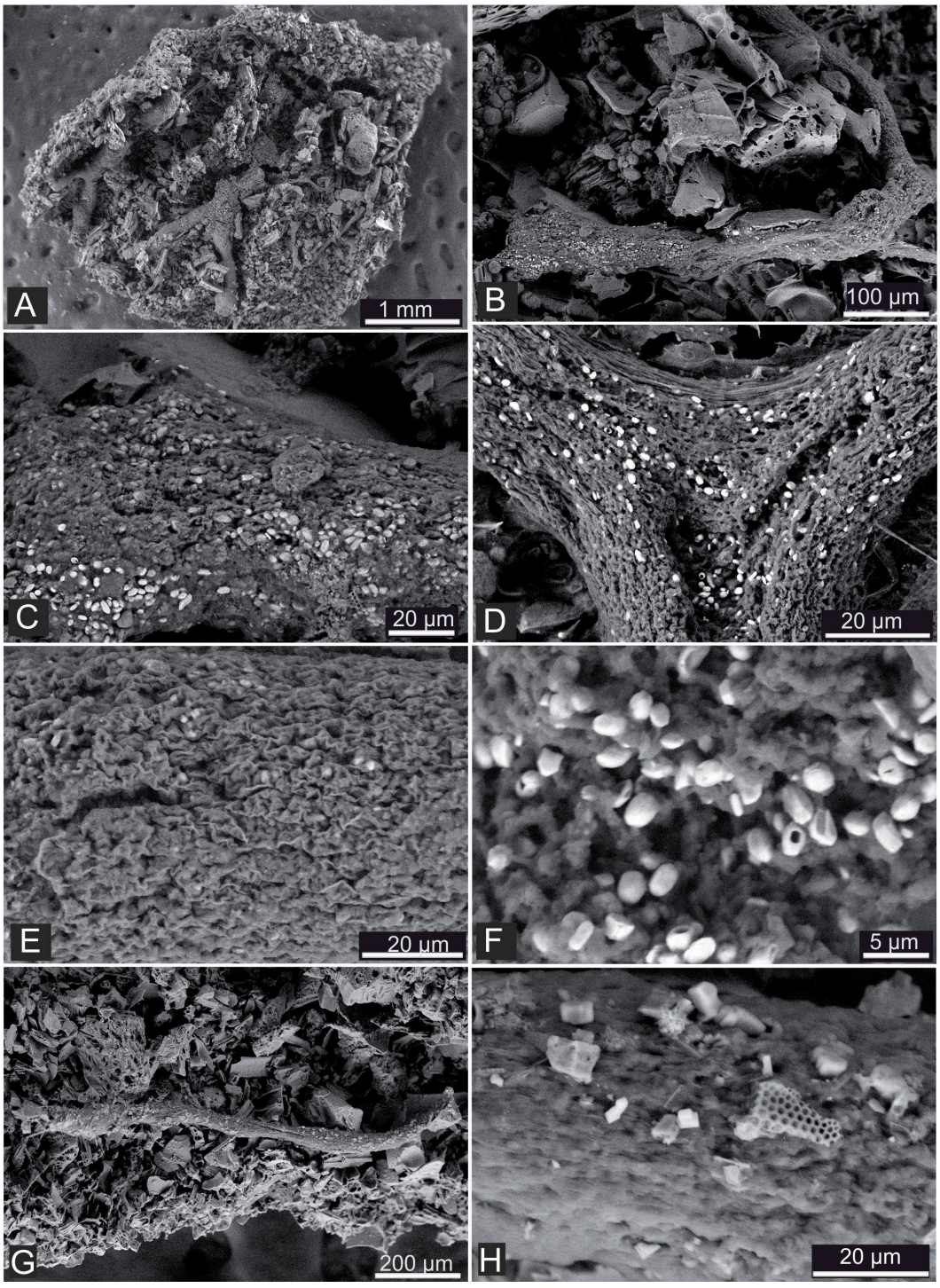


**Fig. 19.** *Laminarena variabilis* gen. et sp. nov., 32.5° N form. SEM images (low vacuum, backscatter mode). **A–E**. Specimen reg. no. TNS Pr714. **A**. Inner surface of fragment with partitions and stercomare. **B–E**. Granellare strand. **B**. Overview of strand. **C–D**. closer view of surface of granellare with areas of exposed barite crystals, apparently where the thin granellare tube has ruptured. **E**. Detail of granellare surface; the organic-walled tube appears crinkled but intact, obscuring any crystals that might be present beneath. **F**. Detail of barite crystals; note that a few have deep shadowed depressions. **G–H**. Specimen reg. no. TNS Pr697. **G**. Overview, including granellare strand. **H**. Detail of surface with the granellare tube apparently intact.

**Granellare and stercomare**

The dissected fragment of specimen TNS Pr714 contained stercomare and granellare, both in good condition (Fig. 18F–G). The stercomare formed several discrete, dark-grey, sausage-shaped masses situated between indistinct ridges that would have formed incomplete radial partitions when the specimen was intact. The masses have the following dimensions: lengths 0.63–2.20 mm (mean 1.23 ± 0.65 mm, n = 6), width 0.20–0.45 mm (mean 0.35 ± 0.07 mm, n = 10), with one longer, branched strand (length at least 3.9 mm), the broken end of which extends beyond the edge of the fragment. The individual stercomata are generally between 8 and 20 μm (mean 14.1 ± 3.24 μm, n = 10) in size (Supp. file 2: Fig. S13C–D). The granellare branches are whitish and lay alongside the stercomare for much of their length (Fig. 18F–G). The main branches are 40–98 μm (mean 65.8 ± 14.9 μm, n = 18) wide; in places, they appear to be closely associated with the stercomare (Fig. 18H). Stercomare masses and granellare branches with similar characteristics were present in a partially dissected fragment of specimen TNS Pr697 (Fig. 18I).

SEM images of granellare from specimen TNS Pr714 show that intracellular barite crystals are present (Fig. 19C–F). They have a generally oval, sometimes hexagonal morphology and resemble the crystals seen in the 30° N form. Their abundance appears to be quite variable along a granellare strand, with dense concentrations in a few places, sparser numbers or a virtual absence of crystals elsewhere. The dense concentrations are associated with areas where the granellare tube had apparently ruptured. In contrast, only a few could be seen where the tube appeared intact and was strongly crinkled, presumably an artifact of drying (Fig. 19E). However, the crystals probably appear to be sparse in such areas only because our view of the cytoplasm is obscured by the granellare tube wall.

Granellare fragments from specimens TNS Pr697 were also observed by SEM (Fig. 19G–H). Unfortunately, because they had not been washed adequately, many parts were obscured by salt crystals. Where the granellare surface could be seen clearly, there was no sign of obvious barite crystals within the cytoplasm, although it was not possible to establish whether they were absent or present but obscured by the granellare tube.

**Molecular characterisation**

*Laminarena variabilis* gen. et sp. nov. is supported by 89% BV and branches as sister to a clade containing representatives of the genera *Aschemonella*, *Abyssalia* Gooday & Holzmann, 2020, *Psammina*, *Galatheammina* Tendal, 1972 and *Moanammina* Gooday & Holzmann, 2020. The branching of the latter clade with *L. variabilis* is not supported by BV. The sequenced 18S barcoding fragment of *L. variabilis* contains 1013–1015 nucleotides and the GC content ranges from 36% to 37%.

**Remarks**

The undescribed xenophyophore specimens that were the subject of Tsuchiya & Nomaki's (2021) feeding experiments came from the same 30° N site as the typical form of *Laminarena variabilis* gen. et sp. nov. described here and clearly belong to the same morphospecies. A remarkably similar morphotype was photographed (but not collected) in the western CCZ, 7362 km to the southeast of our sampling site (Gooday *et al.* 2020b: fig. 1f therein). Kamenskaya *et al.* (2013: fig. 5c, f therein) published in situ photographs of similar specimens from the central CCZ. Probably the morphologically closest described species is *Reticulammina plicata* Gooday, 1996 from 4613 m depth on the Cape Verde abyssal plain in the NE Atlantic (Gooday 1996). The unique specimen consists of the thin, undulating plates with sinuous margins and several branches although unlike those of the new species, a few wide reticulations are also present. Concentric zones are visible and broken plate edges show signs of partitions that traverse the zones at right angles, although these appear to have no surface expression. Some rather similar but undescribed xenophyophores have been collected on east Pacific seamounts (e.g., Levin *et al.* 1986: fig. 1e therein; Levin & Thomas 1988: fig. 2c therein).

In terms of test morphology, the 32.5° N form has a more disorganised appearance compared to the rather elegant typical form from 30° N. Instead of broad, sinuous plates, the test comprises much slenderer elements that radiate outwards, widening to varying extents but mainly towards their upper ends. They sometimes branch and a few are punctuated by open spaces. The surface pattern of concentric zones and radial lineations is much less obvious than in the typical form. However, to some extent, specimen TNS Pr703 from 30° N bridges the morphological gap between the two morphotypes. This specimen has a more complicated test than others from the type locality and appears rather more similar to the 32.5° N form, particularly when the seafloor photographs (Supp. file 2: Figs S6E, S10A, C, E) are compared.

Despite their morphological differences, genetic data support the placement of the two forms in the same species. The molecular distance of partial 18S rRNA sequences between specimens from 30° N and 32.5° N is <0.0089 in the Jukes-Cantor model (Jukes & Cantor 1969), and the foraminifera-specific 37f hypervariable regions are almost identical (>99 %), categorizing them as the same species according to the criteria for foraminiferal meta-18S that classifies sequences diverging by less than 1% as conspecifics (Nguyen *et al*. 2023). Since there has been some diversification, we conducted an Approximately Unbiased test for phylogenetic tree selection (Shimodaira 2002). However, with only three sequenced specimens available to analyse, this failed to reveal any evolutionary scenario (data not shown). More information is clearly required in order to resolve phylogenetic relationships within this species.

It is not obvious why the 30° N and 32.5° N forms have diverged so much in terms of morphology, or whether there are any environmental drivers that are responsible for the differences between them. As noted above, bottom topography is similar between the two areas, but some environmental differences have been detected (Nomaki unpubl. data). At the 30° N site, CN ratios were higher, and carbon isotopic compositions ($\delta^{13}C$) were lower than at 32.5° N, suggesting that the sedimentary organic matter was probably more refractory and may have originated from a different source. This may explain the lower prokaryotic cell numbers and porewater $[NH]^{+}$ concentrations at 30° N compared to 32.5° N, despite TOC concentrations being comparable or even higher. If food is of lower quality at the more southerly site, this would be consistent with the test morphology of the typical form of *Laminarena variabilis* gen. et sp. nov., which seems better adapted for particle trapping than the more northerly form. Further analysis is needed in order to understand the factors responsible for the striking morphological differences between these two genetically similar xenophyophore populations.

There are precedents for morphological differences between genetically similar populations of xenophyophores that are separated geographically. Two species from the western CCZ, *Aschemonella monilis* Gooday & Holzmann, 2017 and *Moanammina semicircularis* Gooday & Holzmann, 2017, yielded sequences identical to those obtained from specimens collected in the eastern CCZ (Gooday *et al.* 2020a), although in these cases the geographical separation was 3800 km, compared to only 270 km between the two forms of *Laminarena variabilis* gen. et sp. nov.

### *Pebble-shaped, honeycombed xenophyophore* *(Fig. 20)*

#### Material examined

NW PACIFIC OCEAN – **32.5° N** • 1 spec., 32°34.8′ N, 143°46.2′ E; depth 5505 m; 22 Oct. 2022; H. Nomaki leg.; Dive 1659 of HOV *Shinkai 6500*, core Red#8; National Museum of Nature and Science, Tsukuba, Japan, reg. no. TNS Pr696.

#### Description and remarks

As seen through the side of the core tube, the test resembles a large, ovate pebble and was not initially recognised as an organism (Fig. 20A–B). Based on μCT scans, it measures 27 mm long, 22 mm wide and 21 mm high with a roughly circular cross section. The test is finely granular and composed of small grains, most of them probably mineral particles, although some that are more rounded may be radiolarians. The surface is raised into low, contiguous bumps, measuring 1.3–2.3 mm (mean 1.75 ± 0.25 mm) in

maximum diameter, best seen in oblique lighting (Fig. 20C). They are developed to varying degrees across the surface, although partially obscured on the upper part by a dusting of fine sediment that was resuspended during sampling. In several places, notably at one end where these bumps are particularly obvious, several have been damaged, revealing hollow interiors (Fig. 20D).

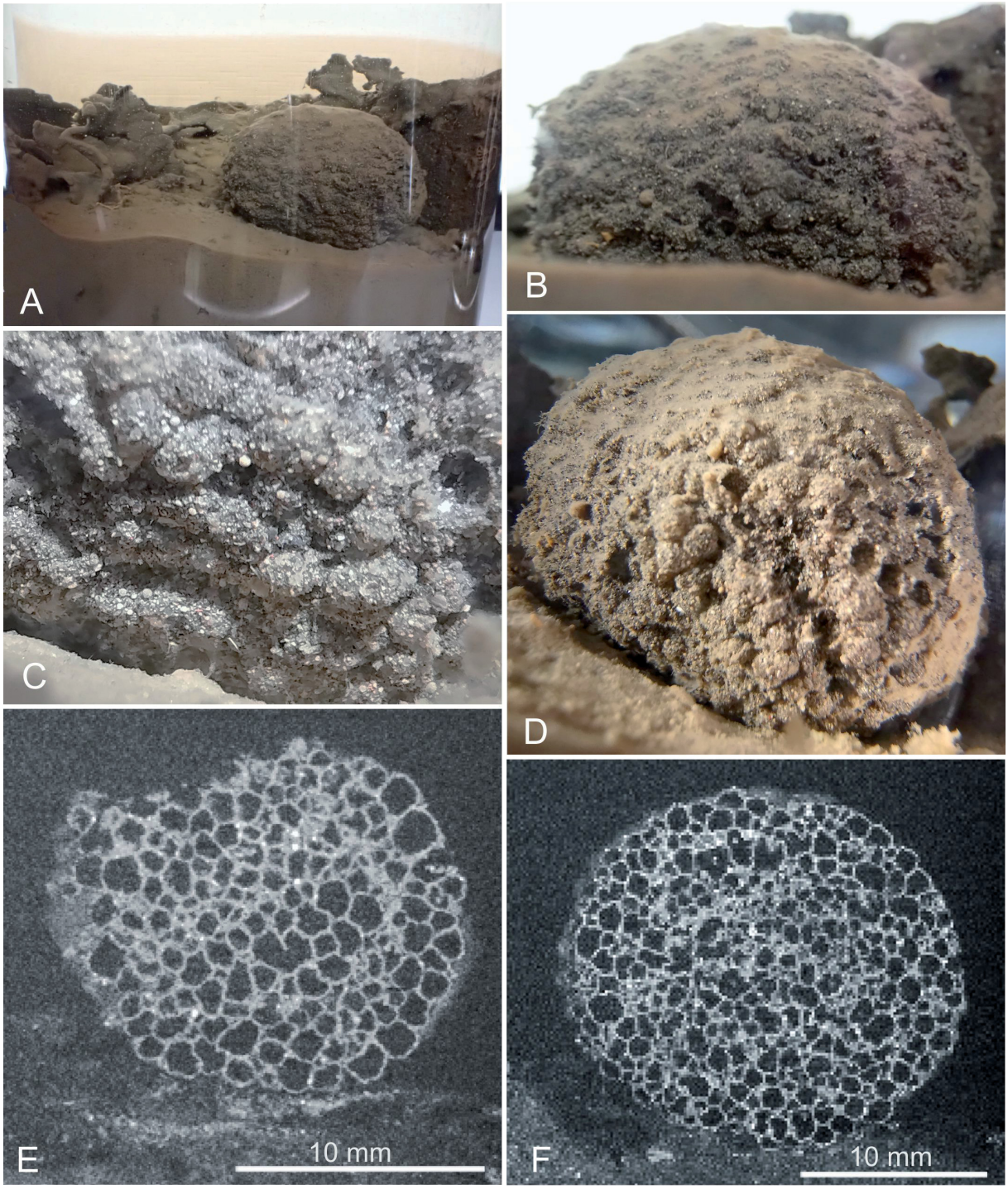


**Fig. 20.** 'Pebble-shaped, honeycombed xenophyophore', specimen reg. no. TNS Pr696. **A–D**. Photographs of intact test taken from different angles through the wall of the core tube. **E–F**. Micro-CT slices showing compartmentalised interior of the test.

In μCT renders, the test is seen resting on the core surface with no obvious structures extending into the sediment (Fig. 20E–F). The interior resembles a honeycomb. It is completely occupied by small cell-like compartments of varying sizes (0.9–2.0 mm; mean 1.64 ± 0.33 mm, n = 14) but with larger compartments tending to occur around the periphery. Apart from some that are smaller, the cells appear to be empty.

Although the nature of this curious organism cannot be confirmed because the test was not removed from the core, it is most likely a novel xenophyophore. The division of the interior into small compartments is reminiscent of the internal structure of *Psammina multiloculata* Kamenskaya, Gooday & Tendal, 2015 (Kamenskaya *et al*. 2015) and an undescribed species of *Psammina* of Gooday *et al.* (2024), both from the eastern half of the CCZ. In these species, the interior is partitioned into numerous small concentrically arranged chambers. However, these are plate-like forms in which the compartments form a single layer. A spherical 'xenophyophore mudball' from the western CCZ (Gooday *et al.* 2020a) has a test consisting of compartments arranged in concentric layers. In contrast to this undescribed 'mudball', our present specimen is ovate rather than spherical, larger in overall size with larger compartments that are not arranged concentrically. Moreover, the test shows little sign of damage and appears to be more robust than the very friable CCZ 'mudball'.

### *Other organisms associated with the xenophyophores*

Incidental observations were made of organisms associated with the xenophyophores (Table 2; Fig. 21; Supp. file 2: Fig. S14). Since these could only be seen through the wall of the tube containing the xenophyophores, the inventory should be regarded as incomplete, as well as mainly limited to those

**Table 2.** Organisms and structures made by organisms associated with the two xenophyophore genera studied herein. The specimens were seen on the exterior of the xenophyophore tests, except for the foraminiferan *Spiculosiphon* Christiansen, 1964, which inhabited the sediment around the tests. The TNS registration numbers for individual xenophyophore specimens and the sampling sites (° N) are given at the head of each column.

| | ***Psammina*** spp. | | | ***Laminarena variabilis*** gen. et sp. nov. | | | | | | |
|---|---|---|---|---|---|---|---|---|---|---|
| **Organism** | **Pr691** | **Pr694** | **Pr695** | **Pr714** | **Pr699** | **Pr700** | **Pr702** | **Pr703** | **Pr704** | **Pr697** |
| | **32.5°** | **32.5°** | **32.5°** | **32.5°** | **32°** | **32°** | **32°** | **32°** | **32°** | **32.5°** |
| **Metazoans** | | | | | | | | | | |
| Amphipod | | | | | | | | | | 1 |
| Playhelminth: Egg case | | | | | | | | | 1 | |
| Polychaete: Large tube | | | | 1 | | | | 3 | 1 | |
| Serpulid tube | | | | | | | | | 1 | |
| Narrow erect tube | | | | | | | | 3 | | |
| Larger low dome | | | | | | | | 1 | | |
| Indeterminate | | | | | | | | | 1 | |
| **Foraminifera** | | | | | | | | | | |
| Small white dome | | | | | | | | 3 | | 2 |
| Irregular chamber | | | | | | | | 1 | | |
| Large white patch | | | | | | 1 | 1 | | | |
| ? *Spiculosiphon* | 2 | 4–5 | 1 | | | | | | | 3 |

organisms visible on the external surfaces of the xenophyophore tests. Structures made by metazoans included various wide tubes, probably those of polychaetes, several much narrower indeterminate tubes, an indeterminate 'polyp'. and a single white platyhelminth egg case identified as *Fecampia abyssicola* Christensen, 1981, a species already recorded from the NW Pacific by Song *et al.* (2021). The Larger low dome shown in Supp. file 2: Fig. S14D resembles some demosponges (*Tentorium* sp.) from the Clarion Clipperton Zone, illustrated by Lim *et al*. (2024: fig. 1o–p therein). The only actual unambiguous

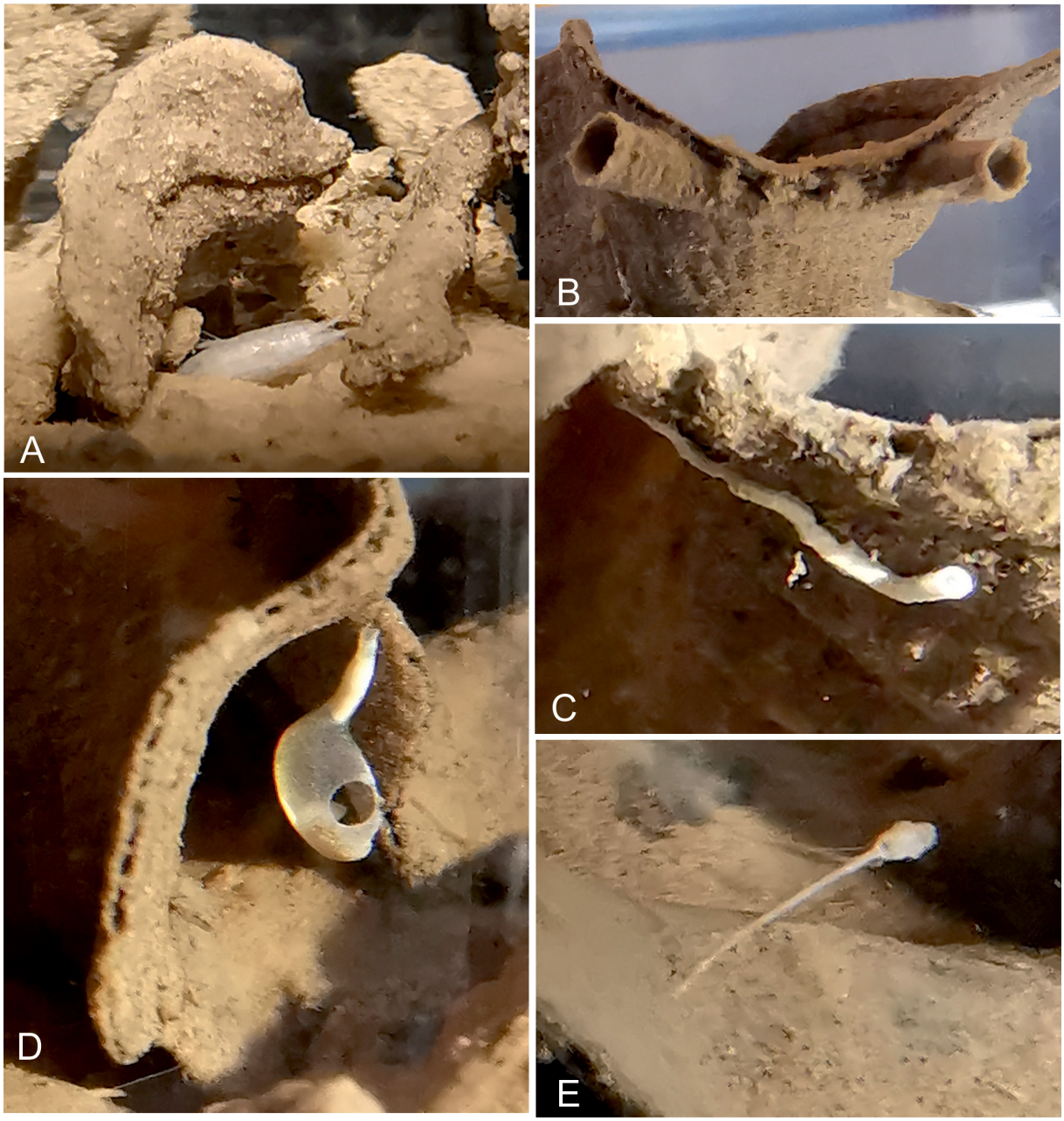


**Fig. 21.** Associated organisms. **A**. *Laminarena variabilis* gen. et sp. nov., 32.5° N form, specimen reg. no. TNS Pr697; amphipod sheltering beneath a plate. **B–E**. *Laminarena variabilis*, typical 30° N form, specimen reg. no. TNS Pr705. **B**. Polychaete tube. **C**. Calcareous polychaete (serpulid) tube. **D**. Cocoon of the platyhelminth *Fecampia abyssicola* Christensen, 1981; the neat hole was possibly made by a gastropod. **E**. Indeterminate 'polyp'.

metazoan was an amphipod that was partly hidden in a fold of *L. variabilis* specimen TNS Pr697. Finally, a single irregularly shaped monothalamid and various whitish domes, at least some of them presumably monothalamid foraminifera, were also present.

In addition to these directly associated organisms, narrow tubes resembling the monothalamid foraminiferal genus *Spiculosiphon* projected vertically from the sediment around some of the xenophyophores (Supp. file 2: Fig. S14F), while μCT renders revealed various likely foraminiferan tubes, both branched and unbranched, within the sediment (notably Figs 3, 10A). Two long, straight, tapered tubes situated close to the holotype of *Psammina yokosukae* sp. nov. (Fig. 3A–B) are probably representatives of the genus *Bathysiphon* Sars, 1872. Finally, we noted the presence of what appear to be feeding marks on *Laminarena variabilis* gen. et sp. nov. specimen TNS Pr703 (Supp. file 2: Fig. S9C).

## Discussion

### Molecular phylogeny

The xenophyophore sequences included in the cladogram and phylogenetic tree (Fig. 1) cluster in six main clades with *Stannophyllum* spp. and *Tendalia reteformis* Gooday & Holzmann, 2017 branching at the base. The monophyly of the following four clades is sustained by bootstrap values: *Psammina* sp. 2 and *Galatheammina* sp. 3 (100% BV). *Shinkaiya lindsayi* and *Reticulammina cerebriformis* Gooday, Aranda da Silva & Pawlowski, 2011 (95% BV), *Syringammina corbicula* Richardson, 2001 and *S. limosa* Voltski, Weiner, Tsuchiya, Kitazato, 2018 (92% BV). *Psammina yokosukae* sp. nov., *P. tenuis* and *P. contorta* sp. nov. (99% BV). On the other hand, a group comprising *Semipsammina mattaeformis* Gooday & Holzmann, 2017, *Claraclippia seminuda* Goooday & Holzmann, 2024 and *Bizarria bryiformis* Gooday & Holzmann, 2017 has no bootstrap support. The sixth and largest clade contains twelve taxa and is also unsupported. It encompasses two subclades. The first includes eight species, *Galatheammina interstincta* Gooday & Holzmann, 2017, *Moanammina semicircularis* Gooday & Holzmann, 2020, *Abyssalia foliformis* Gooday & Holzmann, 2020, *A. sphaerica* Gooday & Holzmann, 2020, *Psammina limbata* Kamenskaya, Gooday & Tendal, 2015, *P. tortilis* Gooday & Holzmann, 2018, *P. rotunda* Gooday & Holzmann, 2018 and *P. microgranulata* Gooday & Holzmann, 2018 and is moderately supported (86%). The remaining four species (*Laminarena variabilis* gen. et sp. nov., *Aschemonella aspera* Gooday & Holzmann, 2017, *A. monilis* Gooday & Holzmann, 2017, *A. ramuliformis* Brady, 1884) make up the second subclade, which is not supported.

Species represented by two or more sequences are supported by high bootstrap values (85–100%) except for *Stannophyllum zonarium*, which is sustained by a moderate BV (78%). The sequences obtained from the two specimens of *Psammina yokosukae* sp. nov. build a monophyletic group, but this has no BV support. However, the branching of *P. yokosukae* and *P. tenuis* is moderately supported (86%) and the branching of the latter two species with *P. contorta* sp. nov. has very high BV support (99%). This species grouping can therefore be regarded as stable.

### Wider comparisons

Xenophyophores with tests composed of curved or undulating plate-like elements without reticulations are sometimes seen in seabed photographs from the abyssal Pacific (>4000 m depth). As already mentioned, *Psammina yokosukae* sp. nov. and *P. contorta* sp. nov. are genetically very close to *P. tenuis* from the CCZ and *P. yokosukae* is somewhat similar morphologically. The latter species also resembles unidentified plate-like xenophyophores seen in seafloor photographs from the eastern Clarion-Clipperton Zone (CCZ), Area of Particular Scientific Interest 6 (APEI-6) (Simon-Lledó *et al.* 2019a: fig. 10a therein), the Russian exploration license area in the more central CCZ (Kamenskaya *et al*. 2013: fig. 5d, f therein), and areas near Kiribati to the west of the CCZ (Simon-Lledó *et al*. 2019c: fig. 3n therein), all located well to the south of the Japanese Archipelago. The closest morphological similarity, however, is between the 30° N

form of *Laminarena variabilis* gen. et sp. nov. and a specimen photographed on the seafloor in APEI-4 of the CCZ (7.0° N, 149.9° W, 5018 m; Gooday *et al*. 2020b: fig. 1f therein). The photograph clearly shows concentric zones and there are vague indications of radial ridges. Although specimens were not collected and we can only point out morphological similarities based on photographs, these comparisons suggest that *L. variabilis* could possibly range across a distance of more than 7000 km. In fact, a geographical range of this magnitude would not be unprecedented. Some other xenophyophore species are reported to have ranges in excess of 10 000 km, again based on morphology (Araya & Gooday 2018), while the longest genetically confirmed range is currently ~3800 km (Gooday *et al*. 2020a).

In contrast, strikingly different test morphologies are displayed by the genetically similar 30° N and 32.5° N morphotypes of *L. variabilis* gen. et sp. nov. which are separated by a mere 271 km. There is currently no obvious explanation for this surprising observation. Nevertheless, it underlines the fact that we still know relatively little about the degree to which test morphology is conserved within xenophyophore species. Tendal (1972) concluded that xenophyophore species usually have characteristic test shapes. This is certainly true in the case of some well-documented species such as *Syringammina fragilissima* Brady, 1883 (Bett 2001; Hughes & Gooday 2004), but apparently not in *L. variabilis*. There is also evidence for morphological differences between geographically separated populations of some other xenophyophore species (Gooday *et al*. 2020a). The test agglutination of the 30° N and 32.5° N morphotypes, however, is much more consistent, as it seems to be in many xenophyophore species (Tendal 1972). Considerations such as these underline the importance of molecular data for establishing geographical ranges for xenophyophore species.

**The *Psammina* problem**

The genus *Psammina* currently encompasses a polyphyletic assemblage of species (Gooday *et al.* 2018). Among those that have been sequenced, the stalked species found on hard substrates appear to form a genetically coherent group (Gooday *et al*. 2018), but others are not closely related (Gooday *et al*. 2017a). Unfortunately, none of the species of *Psammina* described in the earlier literature, including the genotype *Psammina nummulina* Haeckel, 1889 and two others from the equatorial Pacific (Haeckel 1889), has been sequenced. These were described by Tendal (1972) as being "discoidal with large pores along the margin" and composed of "two hard plates" with pillar-like structures between them. The lack of genetic data for the type species makes it impossible to determine which, if any, of the sequenced species represents the true *Psammina* as originally described. The problem is compounded by the fact that the genus now includes a much wider range of morphologies than those of Haeckel's (1889) species. These problems are shared with some other xenophyophore genera, such as *Galatheammina* (Gooday *et al.* 2017a), and make it difficult to construct a higher-level classification of the group that accurately reflects phylogenetic relationships.

Here, we assign our two new species from 32.5° N to this genus because they are placed close in the phylogeny to *Psammina tenuis*. We adopted this pragmatic approach simply in order to minimise confusion. However, we recognise that all three species may eventually require the establishment of a new genus. *Laminarena variabilis* gen. et sp. nov. also displays some *Psammina*-like characteristics, notably the basically plate-like morphology and internal partitions. However, it is clearly distinct genetically from our two species of *Psammina* and from *P. tenuis* and therefore cannot be referred to the same genus.

**Species associations**

A puzzling feature of the small-scale distribution of our xenophyophores is the close physical proximity of two different species within a single pushcore (Fig. 22). Specimen TNS Pr697 of *Laminarena variabilis* gen. et sp. nov. at 32.5° N occurs together with a smooth-walled xenophyophore that will be described separately. Similarly, the unique specimen of the undescribed pebble-like species is found

next to the holotype of *Psammina contorta* sp. nov. Since no genetic data are available for either of these two associates, we cannot unequivocally eliminate the possibility that they represent different stages of the species with which they occur. However, these two morphotypes are so fundamentally different morphologically from *L. variabilis* in one case and *P. contorta* in the other, as well as from each other, that this seems extremely unlikely. It is possible that the species settled independently on organically enriched patches of sediment. Another scenario is that the morphologically complex tests of species such as *P. contorta* trap organic matter, creating conditions that are attractive to other xenophyophores. Complex tests are known to host diverse assemblages of smaller metazoans and protists (Levin & Thomas 1988; Hughes & Gooday 2004), in part because they provide a likely source of food (Levin 1994). It is notable that ophiuroids are often seen curled around the bases of xenophyophore tests (Levin *et al.* 1986), probably because these are places where organic matter accumulates. Although ophiuroids are mobile animals with diets and feeding modes that are different from those of sessile xenophyophores, it is possible that both might benefit from occupying food-rich microhabitats.

**Test morphology and food acquisition**

Levin & Thomas (1988) proposed that the folded or contorted plate-like tests of some xenophyophores, in their case from east Pacific seamounts, acted as traps for particles carried by passing currents. If some particles are organic, then particle trapping will provide the xenophyophores with a concentrated source of food that could be captured by pseudopodia deployed from the raised margins of the test. The xenophyophores described here, particularly the typical 30° N form of *Laminarena variabilis* gen. et sp. nov., would seem ideally suited to this mode of feeding. Tsuchiya & Nomaki (2021) conducted in situ feeding experiments on two individuals of this species at a location <400 m away from our 30° N sampling site and only 4 m deeper. They found that both specimens utilised $^{15}$N-labeled diatoms, representing particulate organic matter such as phytodetritus, as well as taking up dissolved organic matter.

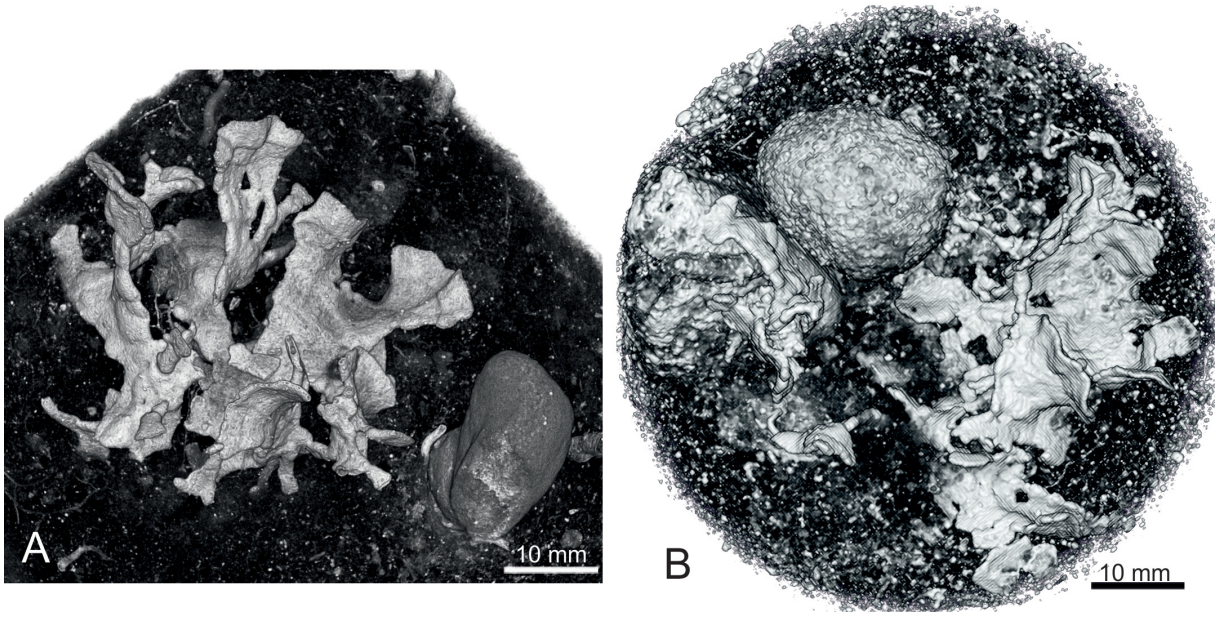


**Fig. 22.** Associations between xenophyophores within two cores from the 32.5° N, as seen in μCT renders (views from above), showing exterior surfaces. **A**. Core with *Laminarena variabilis* gen. et sp. nov., 32.5N form, reg. no. TNS Pr697 and undescribed smooth-walled xenophyophore. **B**. Core with *Psammina contorta* sp. nov., paratype, reg. no. TNS Pr694 and undescribed pebble-like xenophyophore (TNS Pr696).

Interestingly, some bryozoan colonies display morphologies that are remarkably similar to those of some epifaunal xenophyophores. In particular, species in the bryozoan genus *Reteporella* Busk, 1884 closely resemble tests of *L. variabilis* gen. et sp. nov. in terms of overall morphology (e.g., Rauschert & Arntz, 2015), although the plates themselves have a perforated lattice-like structure. Bryozoans are colonial suspension feeding animals that can actively generate feeding currents, whereas xenophyophores have no obvious means of doing this. However, the morphological parallels between these xenophyophores and certain bryozoan colonies may reflect some common adaptations for acquiring food.

**Compartmentalisation of the test**

Two of our species, *Laminarena variabilis* gen. et sp. nov. and the undescribed pebble-shaped morphotype, have clearly developed internal compartments. Micro-CT scans of our two new *Psammina* species reveal indications of internal compartments, although these are less obvious in broken fragments. As already mentioned, a division of the test interior into small compartments is seen in some other xenophyophore species, notably *Psammina multiloculata*, an undescribed species of *Psammina*, and a spherical 'xenophyophore mudball' (Kamenskaya *et al.* 2015; Gooday *et al.* 2020a, 2024). In several other species of *Psammina* the test interior is subdivided by bars that traverse the width of the test. These include *P. zonaria* (Tendal 1994) and *P*. aff. *limbata* Form 2 of Gooday *et al.* (2018). The most extreme example of compartmentalisation is provided by the test of *Aschemonella monilis.* This comprises a series of overlapping chambers with tiny pore-like openings between them that also serve as apertures on the final chamber (Gooday *et al.* 2017b).

It seems likely that these compartments perform different functions in different species. In *P. zonaria* and notably *L. variabilis* gen. et sp. nov., the partitions probably serve to strengthen the delicate test structure. In the latter case they also seem to provide channels directing the growth of the granellare and stercomare strands that run through them, perhaps providing support for these 'soft' structures. In reef-dwelling larger calcareous foraminifera, compartments are used to harbour symbiotic algae (Lee *et al*. 2006), suggesting that similar features in xenophyophores could possibly contain bacterial symbionts. However, there is no evidence to support this highly speculative idea.

## Acknowledgements

We thank the captain and crew of RV *Yokosuka*, as well as the HOV *Shinkai 6500* team, for their great help in collecting the specimens used herein during the relevant research expeditions, and Kaya Oda for her help during sample handling and observations. This work was partly supported by the Japan Society for the Promotion of Science (JSPS) funding P21729 and 21H01202 and the Ocean Shot Research Grant Program "MEIODYSSEA". We are grateful to the three anonymous reviewers for their comments, which helped to improve the manuscript, and particularly to Reviewer 3 (Ivan Voltski), who provided a very thorough critique of the text and figures and offered many valuable suggestions that made us think again about aspects of the species descriptions.

## References

Amon D.J., Ziegler A., Dahlgren T., Glover A.G., Goineau A., Gooday A.J., Wiklund H. & Smith C.R. 2016. Insights into the abundance and diversity of abyssal megafauna in a polymetallic-nodule region in the eastern Clarion-Clipperton Zone. *Scientific Reports* 6: 30492. https://doi.org/10.1038/srep30492

Araya J.F. & Gooday A.J. 2018. First record of a xenophyophore (Rhizaria: Foraminifera) on the Chilean Margin. *Zootaxa* 4455: 589–592. https://doi.org/10.11646/zootaxa.4455.3.16

Bett B.J. 2001. UK Atlantic Margin Environmental Survey: introduction and overview of bathyal benthic ecology. *Continental Shelf Research* 21: 917–956. https://doi.org/10.1016/S0278-4343(00)00119-9

Durden J.M., Bett B.J., Jones D.O.B., Huvenne V.A.I. & Ruhl H.A. 2015. Abyssal hills – hidden source of increased habitat heterogeneity, benthic megafaunal biomass and diversity in the deep sea. *Progress in Oceanography* 137: 209–218. https://doi.org/10.1016/j.pocean.2015.06.006

Fujioka K., Watanabe M. & Kobayashi K. 1989. Deep-sea photographs of the northwestern and central Pacific Ocean – an invitation to deep-sea environment. *Bulletin of the Ocean Research Institute, University of Tokyo* 27: 1–214.

Gooday A.J. 1996. Xenophyophores (Protista) including two new species, from two abyssal sites in the Northeast Atlantic Ocean. *Journal of Foraminiferal Research* 26: 193–208. https://doi.org/10.2113/gsjfr.26.3.193

Gooday A.J. & Wawrzyniak-Wydrowska B. 2023. Macrofauna-sized foraminifera in epibenthic sledge samples from five areas in the eastern Clarion-Clipperton Zone (equatorial Pacific). *Frontiers in Marine Science* 9: e1059616. https://doi.org/10.3389/fmars.2022.1059616

Gooday A.J., Holzmann M., Caulle C., Goineau A., Kamenskaya O.E., Weber A.A.-T. & Pawlowski J. 2017a. Giant protists (xenophyophores, Foraminifera) are exceptionally diverse in parts of the abyssal eastern Pacific licensed for polymetallic nodule exploration. *Biological Conservation* 207: 106–116. https://doi.org/10.1016/j.biocon.2017.01.006

Gooday A.J., Holzmann M., Caulle C., Goineau A., Jones D.O.B., Kamenskaya O.E., Simon-Lledó E., Weber A.A.-T. & Pawlowski J. 2017b. New species of the xenophyophore genus *Aschemonella* (Rhizaria: Foraminifera) from areas of the abyssal eastern Pacific licensed for polymetallic nodule exploration. *Zoological Journal of the Linnean Society* 182: 479–499. https://doi.org/10.1093/zoolinnean/zlx05

Gooday A.J., Holzmann M., Goineau A., Kamenskaya O., Melnik V.F., Pearce R.B., Weber A.A-T. & Pawlowski J. 2018. Xenophyophores (Rhizaria, Foraminifera) from the Eastern Clarion-Clipperton Zone (equatorial Pacific): the genus *Psammina. Protist* 169: 926–957. https://doi:10.1016/j.protis.2018.09.003

Gooday A.J., Durden J.M., Holzmann M., Pawlowski J. & Smith C.R. 2020a. Xenophyophores (Rhizaria, Foraminifera), including four new species and two new genera, from the western Clarion-Clipperton Zone (abyssal equatorial Pacific). *European Journal of Protistology* 75: 125715. https://doi.org/10.1016/j.ejop.2020.125715

Gooday A.J., Durden J.M. & Smith C.R. 2020b. Giant, highly diverse protists in the abyssal Pacific: vulnerability to impacts from seabed mining and potential for recovery. *Communicative and Integrative Biology* 13: 189–197. https://doi.org/10.1080/19420889.2020.1843818

Gooday A.J., Holzmann M., Barrenechea-Angeles I., Lim S.-C. & Pawlowski J. 2024. New xenophyophores (Foraminifera, Monothalamea) from the eastern Clarion-Clipperton Zone (equatorial Pacific). *Zootaxa* 5419: 151–188. https://doi.org/10.11646/zootaxa.5419.2.1

Gouy M., Guindon S. & Gascuel O. 2010. SeaView version 4: a multiplatform graphical user interface for sequence alignment and phylogenetic tree building. *Molecular Biology and Evolution* 27: 221–224. https://doi.org/10.1093/molbev/msp259

Guindon S., Dufayard J.F., Lefort V., Anisimova M., Hordijk W. & Gascuel O. 2010. New algorithms and methods to estimate maximum-likelihood phylogenies: assessing the performance of PhyML 3.0. *Systematic Biology* 59: 307–321. https://doi.org/10.1093/sysbio/syq010

Haeckel E. 1889. Report on the deep-sea Keratozoa collected by H.M.S. Challenger during the years 1873–1876. *Challenger Reports* 32: 1–92. https://doi.org/10.5962/bhl.title.3968

Holzmann M. 2024. Isolation, DNA extraction, amplification and gel electrophoresis of single-celled nonmarine foraminifera (Rhizaria). *In*: Amaresan N. & Chandarana K.A. (eds) *Practical Handbook on Soil Protists*: 181–188. Springer-Verlag, New York. https://doi.org/10.1007/978-1-0716-3750-0_31

Hori S., Tsuchiya M., Nishi S., Arai W., Yoshida T. & Takami H. 2013. Active bacterial flora surrounding foraminifera (Xenophyophorea) living on the deep-sea floor. *Bioscience Biotechnology Biochemistry* 77: 381–384. https://doi.org/10.1271/bbb.120663

Hughes J.A. & Gooday A.J. 2004. The influence of dead *Syringammina fragilissima* (Xenophyophorea) tests on the distribution of benthic foraminifera in the Darwin Mounds region (NE Atlantic). *Deep-Sea Research I* 51: 1741–1758. https://doi.org/10.1016/S0967-0637(04)00112-8

Jukes T. H. & Cantor C.R. 1969. Evolution of protein molecules. *In*: Munrow H.M. (ed.) *Mammalian Protein Metabolism*: 21–132. Academic Press, New York.
https://doi.org/10.1016/B978-1-4832-3211-9.50009-7

Kamenskaya O.E., Melnik V.F. & Gooday A.J. 2013. Giant protists (xenophyophores and komokiaceans) from the Clarion-Clipperton ferromanganese nodule field (Eastern Pacific). *Biology Bulletin Reviews* 3: 388–398. https://doi.org/10.1134/S2079086413050046

Kamenskaya O.E., Gooday A.J., Tendal O.S. & Melnik V.F. 2015. Xenophyophores (Protista, Foraminifera) from the Clarion-Clipperton Fracture Zone with description of three new species. *Marine Biodiversity* 45: 581–593. https://doi.org/10.1007/s12526-015-0330-z

Lecroq B., Gooday A.J., Tsuchiya M. & Pawlowski J. 2009. A new genus of xenophyophores (Foraminifera) from Japan Trench: morphological description, molecular phylogeny and elemental analysis. *Zoological Journal of the Linnean Society* 156: 455–464.
https://doi.org/10.1111/j.1096-3642.2008.00493.x

Lee J.J. 2006. Algal symbiosis in larger foraminifera. *Symbiosis* 42: 63–75.

Lefort V., Longueville J.E. & Gascuel O. 2017. SMS: Smart Model Selection in PhyML. *Molecular Biology and Evolution* 34: 2422–2424. https://doi.org/10.1093/molbev/msx149

Levin L.A. 1994. Paleoecology and ecology of xenophyophores. *Palaios* 9: 32–41.
https://doi.org/10.2307/3515076

Levin L.A. & Thomas C.L. 1988. The ecology of xenophyophores (Protista) on eastern Pacific seamounts. *Deep-Sea Research Part A. Oceanographic Research Papers* 35: 2003–2027.
https://doi.org/10.1016/0198-0149(88)90122-7

Levin L.A., DeMaster D.J., McCann L.D. & Thomas C.L. 1986. Effects of giant protozoans (class: Xenophyophorea) on deep-seamount benthos. *Marine Ecology Progress Series* 29: 99–104.
https://doi.org/10.3354/meps029099

Lim S.C., Wiklund H., Glover A.G., Dahlgren T.G. & Tan K.S. 2017. A new genus and species of abyssal sponge commonly encrusting polymetallic nodules in the Clarion-Clipperton Zone, East Pacific Ocean. *Systematics and Biodiversity* 15: 507–519. https://doi.org/10.1080/14772000.2017.1358218

Nguyen N., Pawłowska J., Barrenechea Angeles I., Zajaczkowski M. & Pawłowski J. 2023. Metabarcoding reveals high diversity of benthic foraminifera linked to water masses circulation at coastal Svalbard. *Geobiology* 21: 133–150. https://doi.org/10.1111/gbi.12530

Pawlowski J. & Holzmann M. 2014. A plea for DNA barcoding of foraminifera. *Journal of Foraminiferal Research* 44: 62–67. https://doi.org/10.2113/gsjfr.44.1.62

Rauschert M. & Arntz W.E. 2015. *Antarctic Macrobenthos: A Field Guide of the Invertebrates Living at the Antarctic Seafloor*. Wurster Nordseekueste, Germany.

Schultze F.E. 1907. Die Xenophyophoren, eine besondere Gruppe der Rhizopoden. *Wissenschaftliche Ergebnisse der Deutschen Tiefsee-Expedition auf dem Dampfer* "*Valdivia*" *1898–1899* 11: 1–55.
https://doi.org/10.5962/bhl.title.2171

Shimodaira H. 2002. An approximately unbiased test of phylogenetic tree selection. *Systematic Biology* 51: 492–508. https://doi.org/10.1080/10635150290069913

Simon-Lledó E., Bett B.J., Huvenne A.A.I., Schoening T., Benoist N.M.A., Jeffreys R.M., Durden J.M. & Jones D.O.B. 2019a. Megafaunal variation in the abyssal landscape of the Clarion Clipperton Zone. *Progress in Oceanography* 170: 119–133. https://doi.org/10.1016/j.pocean.2018.11.003

Simon-Lledó E., Bett B.J., Huvenne V.A.I., Schoening T., Benoist N.M. & Jones D.O.B. 2019b. Ecology of a polymetallic nodule occurrence gradient: implications for deep-sea mining. *Limnology and Oceanography* 64: 1883–1894. https://doi.org/10.1002/lno.11157

Simon-Lledó E., Thompson S., Yool A., Flynn A., Pomee C., Parianos J. & Jones D.O.B. 2019c. Preliminary observations of the abyssal megafauna of Kiribati. *Frontiers in Marine Science* 6: 605. https://doi.org/10.3389/fmars.2019.00605

Stefanoudis P.V., Schiebel R., Mallet R., Durden J.M., Bett B.J. & Gooday A.J. 2016. Agglutination of benthic foraminifera in relation to mesoscale bathymetric features in the abyssal NE Atlantic (Porcupine Abyssal Plain). *Marine Micropalaeontology* 123: 15–28. https://doi.org/10.1016/j.marmicro.2015.12.005

Song X., Lyu M., Zhang X., Ruthensteiner B., Ahn I.-Y., Pastorino G., Wang Y., Gu Y., Ta K. & Sun J. 2021. Large plastic debris dumps: new biodiversity hot spots emerging on the deep-sea floor. *Environmental Science & Technology Letters* 8 (2): 148–154. https://doi.org/10.1021/acs.estlett.0c00967

Swinbanks D.D. 1982. *Paleodictyon*: the traces of infaunal xenophyophores? *Science* 218: 47–49. https://doi.org/10.1126/science.218.4567.47

Swinbanks D.D. & Shirayama Y. 1986a. High levels of natural radionuclides in a deep-sea infaunal xenophyophore. *Nature* 320: 354–357. https://doi.org/10.1038/320354a0

Swinbanks D.D. & Shirayama Y. 1986b. A model of the effects of an infaunal xenophyophore on $Pb^{210}$ distribution in deep-sea sediments. *La Mer* 24: 69–74.

Tendal O.S. 1972. A monograph of the Xenophyophoria. *Galathea Report* 12: 7–103.

Tendal, O.S. 1973. Xenophyophoria from the collections of the R/V "Vitiaz". *Akadamie Nauk USSR* 12: 25–30. [In Russian.]

Tendal O.S. 1994. Protozoa Xenophyphorea Granuloreticulosa: *Psammina zonaria* sp. nov. from the West Pacific and some aspects of the growth of xenophyophores. *In*: Crosnier A. (ed.) Résultats des Campagnes MUSORSTOM 12. *Mémoires du Muséum national d'Histoire naturelle, Série A, Zoologie* 161: 49–54. Available from https://www.biodiversitylibrary.org/page/58753949 [accessed 9 May 2025].

Tendal O.S. 1996. Synoptic checklist and bibliography of the Xenophyophorea (Protista), with a zoogeographical survey of the group. *Galathea Report* 17: 79–101.

Tendal O.S., Swinbanks D. & Shirayama Y. 1982. A new infaunal xenophyophore (Xenophyophorea, Protozoa) with notes on its ecology and possible trace fossil analogs. *Oceanologica Acta* 5: 325–329.

Tsuchiya M. & Nomaki H. 2021. Rapid response of the giant protist xenophyophores (Foraminifera, Rhizaria) to organic matter supply at abyssal depths revealed by an *in situ* dual stable isotope labelling experiment. *Deep-Sea Research I* 176: 103608. https://doi.org/10.1016/j.dsr.2021.103608

Voltski I., Weiner A., Tsuchiya M. & Kitazato H. 2018. Morphological and genetic description of *Syringammina limosa* sp. nov., the first xenophyophore (Foraminifera) from the deep Sea of Okhotsk,. *Deep-Sea Research II* 154: 32–46. https://doi.org/10.1016/j.dsr2.2017.12.001

Printed versions of all papers are deposited in the libraries of four of the institutes that are members of the *EJT* consortium: Muséum national d'Histoire naturelle, Paris, France; Meise Botanic Garden, Belgium; Royal Museum for Central Africa, Tervuren, Belgium; Royal Belgian Institute of Natural Sciences, Brussels, Belgium. The other members of the consortium are: Natural History Museum of Denmark, Copenhagen, Denmark; Naturalis Biodiversity Center, Leiden, the Netherlands; Museo Nacional de Ciencias Naturales-CSIC, Madrid, Spain; Leibniz Institute for the Analysis of Biodiversity Change, Bonn – Hamburg, Germany; National Museum of the Czech Republic, Prague, Czech Republic; The Steinhardt Museum of Natural History, Tel Aviv, Israël.

## Supplemental material

**Supp. file 1.** Supplementary Table 1. Clone, isolate and accession numbers for species included in Fig. 1. https://doi.org/10.5852/ejt.2025.1004.2973.13385

**Supp. file 2.** Supplementary Figures S1–S14 and captions.
https://doi.org/10.5852/ejt.2025.1004.2973.13389

**Supp. file 3.** Supplementary video 1. Micro-CT scan of *Psammina yokosukae* sp. nov., holotype, reg. no. TNS Pr691. https://doi.org/10.5852/ejt.2025.1004.2973.13391

**Supp. file 4.** Supplementary video 2. Micro-CT scan of *Psammina contorta* sp. nov., holotype, reg. no. TNS Pr695. https://doi.org/10.5852/ejt.2025.1004.2973.13393

**Supp. file 5.** Supplementary video 3. Micro-CT scan of *Laminarena variabilis* gen. et sp. nov., holotype, reg. no. TNS Pr700. https://doi.org/10.5852/ejt.2025.1004.2973.13395

**Supp. file 6.** Supplementary video 4. Micro-CT scan of *Laminarena variabilis* gen. et sp. nov., paratype, reg. no. TNS Pr699. https://doi.org/10.5852/ejt.2025.1004.2973.13397